Title: Internal limiting membrane disruption facilitates engraftment of transplanted human stem cell derived retinal ganglion cells

Running Title: ILM disruption enables RGC engraftment

Authors: Erika A Aguzzi,[1] Kevin Y Zhang,[1,2] Arumugam Nagalingam,[1] Sarah Quillen,[1] Shreya Hariharakumar,[1] Nitin Chetla,[1] Salaheddine Madhoun,[1] Malia M Edwards,[1] Harry A Quigley,[1] Donald J Zack,[1,3] Thomas V Johnson[1,4]

Affiliations:
[1] Wilmer Eye Institute, Johns Hopkins University School of Medicine, Baltimore, Maryland
[2] Department of Pathology, Johns Hopkins University School of Medicine, Baltimore, Maryland
[3] Departments of Neuroscience, Molecular Biology and Genetics, and Genetic Medicine, Johns Hopkins University School of Medicine, Baltimore, Maryland
[4] Cellular and Molecular Medicine Program, Johns Hopkins University School of Medicine, Baltimore, Maryland

Corresponding Author: Thomas V Johnson, MD, PhD. Wilmer Eye Institute, Johns Hopkins University School of Medicine. 400 N Broadway, Smith Bldg, Room M-027. Baltimore, MD, USA. 21287. Email: johnson@jhmi.edu

Acknowledgements: This work was funded by support from: National Eye Institute, National Institutes of Health (K08EY031801 [TVJ]; P30EY001765 [DJZ]); Research to Prevent Blindness (Career Development Award [TVJ] and unrestricted grant support [Wilmer Eye Institute]); The American Glaucoma Society (Young Clinician Scientist Award [TVJ]); The ARVO David L Epstein Award (TVJ and HAQ); The Zenkel Family Foundation; and the Allan & Shelley Holt Rising Professorship in Ophthalmology (TVJ). The authors thank Barbara Smith (JHU Institute for Basic Biomedical Sciences' Microscope Facility) for expert technical assistance with scanning electron microscopy.

Abstract

Retinal ganglion cell (RGC) death causes irreversible vision loss in patients with glaucoma and other forms of optic neuropathy because the mammalian retina and optic nerve lack endogenous regenerative capacity. RGC transplantation and optic nerve regeneration represent a potential translational approach to vision restoration in glaucoma secondary to RGC loss. Functional RGC replacement requires that 1) donor RGCs integrate into the recipient retina and receive synaptic input from afferent bipolar and amacrine cells and that 2) donor RGCs extend their axons and establish synaptic connections to appropriate neurons in the brain. Here, in an effort to address retinal integration, we demonstrate that the internal limiting membrane (ILM) acts as a physical barrier to the integration of transplanted human stem cell-derived RGCs (hRGCs) into the recipient retina following intravitreal transplantation *in vivo*. To circumvent the ILM barrier, we intravitreally injected the nonspecific protease pronase-E in immunosuppressed adult C57BL/6J mice prior to transplantation of hRGCs. Separately, we also transplanted hRGCs into adult *Lama1*^{nmf223} mice, which harbor a point mutation in their *Lama*-α*1* gene that causes developmental ILM dysgenesis. We assessed donor hRGC survival and engraftment using 3D reconstructions of confocal z-stacks in retinal flatmounts. Migration of surviving donor RGC somas into the recipient RGC layer significantly increased after proteolytic or developmental ILM disruption. Moreover, lamination of dendritic arbors into the recipient inner plexiform layer was observed exclusively following ILM disruption. To assess the clinical translatability of this finding, we transplanted hRGCs onto postmortem organotypic human retinal explant cultures and observed significantly increased engraftment following proteolytic ILM digestion. These findings enhance our understanding of the barriers faced by transplanted hRGCs in the adult murine and human retina and provide an avenue for clinically translatable regenerative medicine approaches to vision restoration in optic neuropathy.

1. Introduction

Optic neuropathies cause permanent vision loss as retinal ganglion cells (RGCs) die and their axons, which project visual information to the brain via the optic nerve, degenerate. Glaucoma is the most prevalent optic neuropathy, alone affecting more than 80 million people and representing the world's leading cause of irreversible blindness.[1] As the mammalian retina lacks inherent regenerative capacity,[2] restoring lost vision in patients with optic neuropathy will require development of regenerative approaches to replace functional RGCs within the visual pathway. Neuronal transplantation is a promising approach to restoring function in neurodegenerative disorders.[3-5] Subretinal transplantation of photoreceptors improves vision in models of retinal degeneration[6,7] and is nearing human clinical trial. However, transplanting RGCs has been more challenging, owing to their more complex neurophysiology, reception of complex afferent input from bipolar and amacrine cells in the inner plexiform layer (IPL), and long-distance axonal projections to the brain. Key advancements over the past 15 years have described several efficient methods for generating RGCs from human pluripotent stem cells[8-12] and have identified numerous molecular pathways that can be manipulated to enable the long-distance regeneration of endogenous RGCs from the retrobulbar optic nerve past the chiasm and into key subcortical visual targets.[13-28] In some cases, modulation of these pathways has even produced improvements in rudimentary visually guided behaviors in mice,[26,29] substantiating the premise that establishment of efferent brain connectivity by repopulated RGCs is feasible. However, rigorous demonstrations of synaptogenesis by transplanted RGCs are lacking, and methods to augment this process require further development.

Though transplantation of non-neuronal cells has been trialed to confer neuroprotection to injured endogenous RGCs,[30-33] RGC replacement necessitates transplanting progenitors with neuronal potential or differentiated neurons. Preliminary studies have been successful in documenting rare instances of functional integration by transplanted primary neonatal mouse RGCs,[34] murine stem cell derived RGCs,[35,36] and human stem cell-derived RGCs (hRGCs)[37] in recipient retinas. However, among the relatively few RGCs that survive transplantation (typically <1%),[34-38] even fewer RGCs successfully engraft into the retina by migrating into the host retinal ganglion cell layer (RGCL) and extending dendrites into the inner plexiform layer (IPL), where synaptogenesis with host bipolar and amacrine cells could occur.

One of the challenges of RGC transplantation is that following intravitreal injection, donor cells encounter significant barriers to retinal incorporation. Cell suspensions disperse into an acellular cavity devoid of direct metabolic support. Moreover, the basement membrane at the vitreoretinal interface (the internal limiting membrane, ILM) represents a key obstacle that limits retinal transit of drugs, gene therapy vectors, and cells.[38-40] The ILM is composed of extracellular matrix (ECM) proteins including collagen (type IV, XVIII), laminin, fibronectin, and nidogens 1 and 2.[41,42] During retinal development, ILM recognition by RGCs through integrin receptors is required for appropriate RGCL polarization, migration, and tiling,[43] and ILM-astrocyte interactions modulate glial migration which guides subsequent retinal vascular development.[44,45] However, in adulthood the ILM is not only dispensable, but can serve as a scaffold for the pathological proliferation of fibrocytes, myofibroblasts and glial cells.[46] Indeed, surgical ILM peeling used clinically to relieve vitreomacular traction and can improve vision in patients with macular holes, supporting the feasibility of disrupting or removing the ILM in human patients to augment cell therapy.[47]

It has long been speculated that the ILM might impede retinal integration of intravitreally transplanted RGCs.[48,49] Recently, we provided empirical evidence that proteolytic ILM digestion enables structural integration of hRGCs into co-cultured organotypic mouse retinal explants.[50] Here, extending these findings, we evaluate enzymatic and developmental approaches of ILM disruption for promoting the structural engraftment of transplanted hRGCs in immunosuppressed mice *in vivo* and in human postmortem retinal explant cultures.

Results

ILM disruption through proteolytic and developmental approaches

Previously, we demonstrated that pharmacologic ILM disruption with the proteolytic enzyme pronase-E increased donor hRGC neurite growth into the retinal parenchyma in cultured organotypic retinal explants by ≥40-fold without causing detectable neuro- or gliotoxicity to the host retina.[50] To address whether this approach is also efficacious *in vivo* in disrupting the ILM with minimal off-target effects, we intravitreally administered several doses of pronase (or basic salt solution [BSS], vehicle) in wild type C57BL/6J mice and assessed the retina 2 weeks later (Fig 1A).

The concentration of pronase which yielded successful digestion of the ILM, without causing intraocular hemorrhage or neurotoxicity, was 1.25 U/mL (for lot SLCK2824, or 0.075 U/mL for lot SLCL6671, see *Methods*). Intravitreal pronase concentrations ≤1.5 U/mL caused no gross abnormalities in the retina, whereas concentrations ≥2 U/mL were associated with visible preretinal and intraretinal hemorrhage (Fig 1B), presumably due to digestion of retinal vasculature basement membranes, and similar to our prior observations following intravitreal collagenase administration *in vivo* in rats.[51] Concentrations of ≥6 U/mL caused severe intraocular hemorrhage and gross degradation of the neuroretinal tissue (Fig 1B). Intravitreal pronase (1.25 U/mL) effectively digested the ILM but was not associated with intraocular bleeding or other gross posterior segment abnormalities.

We evaluated the effects of intravitreal pronase on the ILM and the underlying retina in several ways. Immunofluorescent labeling of laminin in BSS-treated retinas exhibited uniform reactivity across the ILM surface, whereas the ILM of pronase-treated retinas contained diffuse full-thickness round defects ranging up to 400 μm^2 in size (Fig 1C, E; Supp Fig 1A, B). Transmission electron microscopy (TEM) demonstrated that the ILM in wildtype animals treated with intravitreal BSS was dense and uniform, with glia abutting the ILM (Fig 1D). In contrast, pronase-treated eyes demonstrated ILM thinning, loss of compaction, irregularity, and frank discontinuities through which glial cells occasionally were noted to protrude (Fig 1D). Scanning electron microscopy (SEM) demonstrated that the ILM surface was continuous and uniform in BSS-treated eyes, whereas pronase induced sizeable craters and holes in the ILM (Fig 1F).

To assess the effects of pronase on resident inner retinal cells, we evaluated neuronal and glial morphology using immunofluorescence. GFAP immunofluorescence in the retinal nerve fiber layer demonstrated modest hypertrophy of astrocytes and Müller glial endfeet following pronase treatment in comparison to BSS injection (Fig 1G; Supp Fig 1A, B), but we did not observe loss of glial cells with pronase 1.25 U/mL as we observed previously with other proteolytic enzymes or high doses of pronase.[50] We quantified the survival of RGC layer neurons (RGCs and displaced amacrine cells labeled with NeuN) and rod bipolar cells (labeled with PKCα) at 2 weeks following intravitreal injection and found that neither cell population was affected by pronase administration (Fig1 H, I). Together these data show that intravitreal pronase administration can be effectively titrated to digest and produce full-thickness defects in the ILM without causing inner retinal neurotoxicity, though modest reactive gliosis was observed.

We considered that proteolytic ILM digestion may confer occult off-target effects on the retina not identifiable on routine histology which could affect RGC engraftment. Therefore, we evaluated RGC transplantation in an independent and complementary model of ILM disruption. *Lama1*^{nmf223} mice harbor a missense mutation in the *Lama-α1* gene which reduces laminin-α1 protein interactions at the N-terminal domain where receptor binding and polymerization motifs are located. These mice exhibit developmental ILM defects associated with ectopic migration of retinal astrocytes into the vitreous cavity, followed by the development of patchy epiretinal gliovascular membranes.[44,45] We reasoned that ILM defects, which permit extravasation of astrocytes from the retina into the vitreous cavity, may also permit migration of intravitreal donor RGCs into the retina.

Before transplanting RGCs in this model, we further characterized the ILM disruption exhibited by these mice. Similar to pronase-treated retinas, laminin immunofluorescence demonstrated full-thickness defects in the ILM of *Lama1*^{nmf223} mice (Fig 1C, E; Supp Fig 1A, C), which were generally sparser than we observed following pronase administration. We also identified a preretinal gliovascular membrane in these mice, as has been described previously (Fig 1C, E; Supp Fig 1A, C).[44,45] TEM demonstrated local breaks in the ILM over diffuse areas of the retinal surface exposing bare glial cells, and in some instances glia projected into the vitreous cavity (Fig 1D). SEM demonstrated that the ILM of *Lama1*^{nmf223} mice contained pits and full-thickness holes, similar to that of pronase-treated retinas (Fig 1F).

Donor hRGC engraftment following ILM disruption

Prior to transplanting hRGCs *in vivo*, we compared the engraftment potential of hRGCs in organotypic retinal explant cultures derived from wildtype C57BL/6J mice to those of *Lama1*^{nmf223} mice (Supp Fig 2A). Similar to our prior work assessing hRGC neurite extension in retinal explant pretreated with pronase or BSS, we observed that tdTomato (tdT) expressing hRGCs[52] survived for at least 7 days in co-culture and that hRGCs on retinas with intact ILM tended to form discrete neuronal clusters (Supp Fig 2B). Further, hRGCs extended robust neurites laterally on the epiretinal surface, but most remained superficial to the retinal parenchyma, and specifically, to the astrocytes within the retinal nerve fiber layer (RNFL) (Supp Fig 2C). A subset of hRGCs exhibited structural engraftment, with cell bodies localized to the RGCL and neurites that grew deeper into and throughout the host neural retina, including the IPL (Supp Fig 2D). Transplantation onto *Lama1*^{nmf223} was associated with an increase in donor hRGC survival (Supp Fig 2E) and a significant increase in the number of donor hRGCs growing neurites into the recipient tissue (Supp Fig 2F).

Having characterized the ILM disruption exhibited following intravitreal pronase administration and in *Lama1*^{nmf223} mice, we next sought to evaluate the effect of ILM disruption on donor hRGC engraftment *in vivo*. We tested both ILM disruption models in parallel, transplanting 3.75x10^5 tdT$^+$ hRGCs into mice immunosuppressed with systemic cyclosporine-A and assessing retinal integration of the graft 2 weeks later (Fig 2A, B). Similar to prior reports,[34,36] hRGCs survived in the majority of eyes (75% of BSS-treated eyes (n=12/16); 80% of pronase-treated eyes (n=32/40); and 95% of *Lama1*^{nmf223} eyes (n=45/50)). The absolute number of surviving hRGCs was generally <1% of the number injected (Fig 2F), commensurate with prior reports.[34-38] There was a modest increase in hRGC survival in pronase-treated eyes compared to BSS-treated eyes, but no increase in *Lama1*^{nmf223} eyes (Fig 2F).

We next characterized the structural engraftment of hRGCs using two primary outcomes: localization of hRGC somas to the endogenous RGCL and lamination of hRGC dendrites within the endogenous IPL. For these studies, we utilized rigorous assessments of high-resolution confocal z-stack 3D renderings of flat-mounted retinas, since transverse sections of the retina would capture only fragments of the hRGC dendrites oriented in the orthogonal plane. Within the host retina, we identified most hRGCs as localized to the epiretinal surface, where the hRGC soma was superficial to the RGCL and astrocytic GFAP processes within the RNFL, which were clearly identified deep to hRGC cell bodies (Fig 2E). In contrast, some hRGCs appeared to have migrated into the RGCL, with a soma that was coplanar to the endogenous RGCL and deep to the astrocytes of the RNFL (Fig 2D). A negligible amount of somal migration into the RGCL was noted in BSS-treated eyes. In contrast, the absolute number and percentages of surviving hRGCs that engrafted were significantly higher in pronase-treated or *Lama1*^{nmf223} eyes (Fig 2I).

To assess the localization of hRGC dendrites in our *in vivo* models, we again analyzed 3D renderings of confocal z-stacks. Individual hRGCs with neurites within the retinal parenchyma were traced and the localization of the neurites was assessed in a retinal layer-specific manner. Unlike our prior observations after transplanting hRGCs onto organotypic retinal explants, wherein donor hRGC neurites appeared to grow throughout the retina in a nonspecific manner,[50] hRGC dendrites transplanted *in vivo* strikingly targeted the IPL for lamination (Fig 2D, G, H, Supp Movie 1: https://www.youtube.com/watch?v=HjkLz_IQJqc; Supp Movie 2: https://www.youtube.com/watch?v=5inRSWuYkoU). In BSS treated eyes, we did not observe hRGCs which had extended dendrites into the IPL, whereas this phenomenon occurred readily in pronase-treated and *Lama1*^{nmf223} eyes (Fig 2J).

While the level of hRGC survival observed in these experiments is comparable to past reports, increasing the survival rates of grafts will be critical to the future translatability of this neuronal transplantation approach. To that end, we wondered whether cyclosporine-A immunosuppression in wildtype mice may have been insufficient in preventing xenograft rejection, and whether that might have contributed to suboptimal hRGC survival. To assess this possibility, we compared transplantation of hRGCs in cyclosporine immunosuppressed C57BL/6J mice to NOD SCID gamma (NSG) mice, which carry mutations in *Prkdc* and *Il2rg* leading to the absence of mature T cells, B cells, and NK cells.[53] We did not identify any improvement in hRGC survival in mice lacking an adaptive immune system (Supp Fig 3), suggesting there is negligible breakthrough adaptive immune rejection of hRGCs in mice systemically immunosuppressed with cyclosporine-A. hRGC death at this relatively early time point is therefore likely to be related to other factors, such as innate immune activity (i.e. by microglia or macroglia) and/or lack of supportive factors in the microenvironment.

Transplantation of hRGCs into human organotypic retinal explants

The translational potential of RGC transplantation necessitates ultimately achieving engraftment into human retinas. However, the structure and composition of the ILM varies among species and also as a function of age.[54] As such, we wondered whether the ILM also obstructs hRGCs from extending dendrites into human retinal tissue, and whether this blockade can be ameliorated with enzymatic ILM digestion. To assess this question, we obtained ocular tissue from human postmortem donors over 70 years of age, isolated their retinas, and cultured them in organotypic fashion. Similar to our prior work with mouse retinal explants,[50] we treated the retinal tissue with a 5 µL droplet of pronase (or BSS, vehicle) onto the inner retinal surface, and then transplanted 1.5×10^5 hRGCs 24h later (Fig 3A). At one week after co-culture, hRGCs survived on the surface of all retinal explants and extended long neurites (Fig 3B), similar to their behavior on mouse retinal tissue (Supp Fig 2B). hRGC survival rates were similar in retinas pre-treated with pronase or BSS (Fig 3D). We again utilized 3D renderings of high magnification confocal z-stacks to evaluate the subcellular localization of hRGCs within the recipient retinal tissue (Fig 3C) and identified a significant increase in the number of hRGCs that elaborated dendrites within the IPL when the ILM was permeabilized with pronase as compared to when the ILM was intact (Fig 3E). These data demonstrate that the ILM inhibits hRGC engraftment into human neural retinas and supports the translational premise of circumventing the ILM for RGC transplantation.

Patterns of donor hRGC dendrite and axonal outgrowth

Having observed hRGC dendrite localization to the retinal parenchyma exclusively following ILM disruption (Fig 4A), we next sought to characterize the dendritic morphology of structurally integrated hRGCs (Fig 4C). We began by tracing engrafted hRGC dendrites within 3D renderings of confocal z-stacks and used volumetric analyses to quantify the percentage and length of dendrites within the major retinal layers. Approximately half of intraparenchymal hRGC dendrites localized within or just deep to the RGCL, while the remaining half localized to the IPL (Fig 4D, E). Unlike in organotypic retinal explants, very few dendrites grew ectopically into the inner nuclear layer (INL) and even fewer were detected in the outer nuclear layer (ONL) (Fig 4D, E).

We next assessed the complexity of hRGC dendritic arbors and compared them to that of mature endogenous mouse RGCs in separate naïve retinas. To do so, we obtained confocal z-stack micrographs of sparsely labeled RGCs in Thy1-YFP mouse retinas, where labeling occurs across an array of RGC subtypes (Fig 4B). Compared to endogenous mouse RGCs, integrated hRGCs had reduced dendrite density and total branch length, but greater average branch length and maximal branch length (Fig 4F). This is consistent with an overall lower dendritic complexity with fewer branch points and more unbranched dendrites. Indeed, Sholl analysis demonstrated that the peak dendritic density occurred closer to the soma in donor hRGCs than endogenous murine RGCs, with a substantially lower overall dendritic complexity (Fig 4G). Together, these data confirm the relatively immature morphology of donor hRGC dendritic arbors at two weeks post-transplantation and provide a benchmark for assessing the maturation of hRGC dendritic architecture over time.

In addition to numerous branched neurites elaborated for a maximal distance of approximately 200 µm from the soma, hRGCs frequently extended a single lengthy axon that traveled, in some cases, for 2-3mm within the retina (Fig 4H). Remarkably, most of these axons were oriented radially towards the optic nerve head (ONH) (Fig 2C, 4I). Disruption of the ILM was associated with a significant increase in the number of hRGC axons growing toward the ONH, with relatively more such axons identified in *Lama1*^{nmf223} than in pronase-treated retinas (Fig 4K). hRGC axons were observed to descend into the ONH, following the trajectory of the endogenous RNFL as axons enter the optic nerve (Fig 4J, Supp Movie 3: https://www.youtube.com/watch?v=-CA-5tcvSpc). Histological examination of the retrobulbar optic nerve, however, failed to demonstrate hRGC axons within the optic nerve tissue itself (data not shown) suggesting either that axons face an obstacle at the level of the glial lamina blocking their entry into the nerve or that axonal optic nerve entry simply does not occur before 2 weeks post-transplantation.

Protein expression within hRGC neurites

Differentiation of pluripotent stem cells to a RGC phenotype yields a mixed population of cells with relatively immature transcriptional signature, showing only minimal expression of the mature RGC marker RBPMS.[9,55] Transplantation of RGCs is associated with molecular evidence of maturation *in vivo*.[36] Therefore, we sought to assess the molecular phenotype of hRGCs after transplantation. At 2 weeks following transplantation, donor hRGCs uniformly expressed RBPMS, with immunoreactivity being stronger in donor neurons than endogenous murine RGCs (Fig 5A). Donor hRGCs also expressed the RGC-specific transcription factor Brn3a (Fig 5B). These data demonstrate post-transplantation maturation of the donor hRGCs *in vivo*.

We previously noted that hRGCs transplanted onto mouse organotypic retinal explants extended immature neurites which co-expressed dendritic and axonal markers >90% of the time when not engrafted into the tissue. By contrast, almost 25% of hRGC neurites which had engrafted into the retinal parenchyma specified neurite identity, expressing either dendritic or axonal markers, but not both.[50] We therefore sought to determine whether neurite maturation occurred in hRGCs following transplantation *in vivo*. As noted above, many hRGCs extended a single long, linear neurite directed towards the ONH which resembled an axon, as well as several shorter more tortuous neurites which resembled dendrites. Indeed, immunofluorescent triple labeling revealed that the shorter neurites near the cell soma expressed MAP2 (a marker of mature dendrites) but not SMI-312 (a marker of mature axons, Fig 5C) whereas the lengthy neurites running with the RNFL expressed SMI-312 (Fig 5D), but not MAP2. Therefore, donor hRGCs transplanted *in vivo* appear to specify mature dendrites and axons within 2 weeks.

Finally, we sought to determine whether donor hRGCs formed synapses with host inner retinal neurons following transplantation. We immunolabeled flat-mounted retinal tissue with antibodies recognizing presynaptic synaptophysin and postsynaptic PSD-95 and noted extensive colocalization of punctate synaptic machinery within the dendrites of donor hRGCs (Fig 5E).

Assessments for graft-to-host intercellular material transfer

An important consideration when interpreting transplantation results is the possibility of intercellular material transfer, a phenomenon first described in photoreceptor transplantation studies, whereby donor-derived fluorescent markers can be transferred to host neurons and potentially lead to erroneous assumptions of donor cell engraftment.[56-60] To evaluate for potential material transfer of tdT in our hRGC transplants, we first transplanted tdT$^+$ hRGCs into mice ubiquitously expressing GFP under the CAG promoter. All putative hRGCs which were tdT$^+$ were also noted to be GFP-negative, confirming their donor origin (Fig 6A). Further, we immunolabeled retinas from mice that received hRGC transplants with antibodies that specifically recognize human mitochondria (hMito, Fig 6B) or human nuclei (HuNu, Fig 6C) and noted expected patterns of subcellular immunoreactivity in all purported donor hRGCs, again confirming their donor origin. Of note, the localization of hMito to hRGC neurites (Fig 6B) enables clear identification of donor dendrites and axons, in addition to cell bodies.

Discussion

Transplantation of human stem cell-derived RGCs holds potential for restoring vision in an array of optic neuropathies. However, prior work has demonstrated several critical obstacles that hinder the efficacy of this approach for restoring visual pathway function. Here, we identify and overcome a primary barrier to the structural engraftment of intravitreally transplanted hRGCs into the recipient retina. Building on our prior work in organotypic retinal explants, we demonstrate that the ILM prevents most donor hRGCs from migrating into the recipient inner retina and from elaborating dendrites into the IPL, where synaptic input from afferent bipolar and amacrine cells might be established. Using two independent approaches – proteolytic ILM digestion or a developmental model of ILM dysgenesis – we observed significant increases in structural hRGC engraftment into the host murine retina. Moreover, we found that disruption of the ILM in human postmortem retinal tissue similarly augments the engraftment of transplanted hRGCs. Together these data provide a clear target for future work aimed at functionally replacing RGCs within the degenerating visual pathway.

Our work builds on prior studies in the regenerative medicine field. Human embryonic stem cell (hESC) derived RGCs have been transplanted into rat eyes, where somal co-localization with the RGCL was reported but donor cells did not appear to extend neurites 3 weeks post-transplantation.[61] In addition, those donor neurons did not express RBPMS, leaving open the question of whether the donor cells had matured into a functional RGC phenotype. Vrathasha et al.[37] transplanted AAV-GFP labeled human induced pluripotent stem cell-derived RGCs into immunocompetent mice and reported a remarkable degree of survival, dendritic complexity, and light responsivity at 2-5 months following transplantation. In comparison to that study, a critical strength of the current work is the rigorous control experiments to rule out the possibility of intercellular material transfer or leaky labeling with the AAV vector leading to erroneous identification of endogenous murine RGCs as donor-derived neurons. Vanugopalan et al.[34] demonstrated that a small proportion of primary mouse RGCs transplanted into rat recipients with intact ILM appear to survive, attain mature RGC morphology, achieve synaptogenesis, and conduct electrophysiological responses to light stimulation, despite overall low survival rates.[34] Differences in these outcomes might be explained by differences in the donor cell source or the donor and/or recipient species.

A notable strength of the current work is the rigorous histological analyses of hRGC subcellular localization with the host retina, performed in flat-mounted retinas rendered and analyzed in 3D. This approach enabled us to simultaneously evaluate the full extent of hRGC dendritic arbors in the x,y plane while retaining the ability to resolve z positions within specific retinal layers. Critically, prior work has focused exclusively on analyses of retinal sections (which capture only a fragment of horizontally oriented dendritic arbors) or 2D maximal projection images of retinal flatmounts, which provide no discrimination between cells lying on the surface of the retina versus those which may have migrated below the ILM.[34,36,62-64] Studies in pre-clinical models of RGC injury induced by intravitreal injection of N-methyl-D-aspartate (NMDA) or ocular hypertension show dendritic extension into the GCL, which is described as neuronal engraftment.[62] The methods to determine graft localization and engraftment are inconsistent across published literature, however, and some studies suggest that transplanted RGCs that accumulated on the vitreous side of the ILM are considered to have integrated. These inconsistent findings are likely related to non-standardized methodologies of determining cellular localization.[38] In our view, it is insufficient to assess functional integration into the host retinal circuitry without first demonstrating neurite distribution into the deeper layers of the retina, and when possible, the IPL sublamina.[62] The lack of consistent methodology for discerning donor somal coplanarity with the host RGCL, and assessment of integration into the IPL, limits accurate reporting and comparison of transplantation outcomes.

An alternative to intravitreal transplantation of hRGCs has been proposed by Baranov et al.[65] and involves subretinal transplantation of the neuronal graft. By circumventing the ILM altogether, a small number of RGCs can migrate into the inner retina from the subretinal space.

Delivering a guidance signal, such as recombinant stromal cell- derived factor-1 (SDF-1), into the vitreous cavity further enhances the migration of hRGCs towards the RGC layer. However, the ultimate efficiency of this delivery method and whether migrating neurons disrupt the neurocircuitry of the host retina remains to be determined.

By providing a clear experimental avenue for increasing donor hRGC engraftment into the inner retina, we hope to bring the possibility of transplantation-mediated RGC replacement closer to clinical translation. Indeed, ILM peeling performed after pars plana vitrectomy and staining the membrane with indocyanine green or Coomassie blue dye is a widely implemented surgical technique for treatment of the vitreomacular traction, macular hole, and epiretinal membrane.[66,67] However, it is possible that complete local ILM removal may introduce new challenges to hRGC engraftment. Neurodevelopmental studies have established that signaling between RGCs and the ILM is critical for organized patterning of the RGC layer and dendritic projection to the IPL. β1- integrin recognition of ILM is required for RGC organization into a single-celled layer. In the absence of β1-integrin, or Cas adaptor proteins (which signal downstream of integrins), retinal neurons form ectopic cell agglomerations, extravasate past the ILM, and in some ways phenotypically resemble laminin mutants.[68] In addition, loss of laminin $\gamma 3$ is associated with defects in retinal lamination and differentiation of RGCs. As such, cellular permeabilization of the ILM, sub-ILM injections,[69] or laser photoporation[70] may be more advantageous for RGC engraftment than *en bloc* ILM resection. Regardless, the barrier role of the ILM identified here has clear translational applicability RGC transplantation.

In addition to its translational relevance, the work described here provides experimental directions that open several new and critical lines of research related to the functional engraftment of RGCs. Prior work has identified numerous molecular pathways that can be modulated to dramatically enhance the axon regeneration of injured endogenous RGCs through the optic nerve, past the chiasm, and to central subcortical visual targets.[71] However, experiments aimed at connecting donor RGCs to inner retinal neurons and growing their axons into the optic nerve have been hampered by extremely poor engraftment into the retinal parenchyma.[38] We have now established a benchmark for hRGC dendritic lamination within the IPL that can be subject to additional manipulations to enhance the efficiency of the process. Moreover, given the localization of synaptic machinery to hRGC dendrites within the IPL, robust functional assessments of donor neuron connectivity to specific retinal circuits can be explored. Finally, given the spontaneous growth of hRGC axons towards and into the ONH, the development of methods to enhance the extension of axons into the optic nerve and beyond are now within reach. The specific growth of hRGC neurites towards the ONH is intriguing and suggests either that hRGC axons use the existing retinal nerve fiber layer as a conduit (potentially mediated by cell surface receptor interactions) or that a yet-unidentified axonal guidance cue is present in the adult retina.

Despite the advances documented here, many critical hurdles to efficient RGC replacement remain. Low survival of transplanted hRGCs is a pervasive issue and must be improved to yield a viable regenerative therapy. There are at least three likely contributors to donor hRGC cell loss following transplantation that should be addressed in future work. These include cell-intrinsic induction of apoptosis in this relatively delicate cell type, immunological insult to the graft, and lack of appropriate microenvironmental support for the neurons.

Neurons in general are challenging to differentiate, culture, and transplant. They are dependent on a highly regulated extracellular microenvironment, which is established *in vivo* by supportive glia, but must be established experimentally in transplantation paradigms. RGCs are vulnerable to injury of subcellular compartments including dendrites and axons, which are likely to be damaged during purification and preparation for transplantation. Indeed, detachment of cells from growth substrates (termed *anoikis*) triggers caspase-8 dependent apoptosis,[72] and may contribute to early cell death following transplantation. Neuroprotective strategies to prevent RGC death from a range of insults have identified numerous cell intrinsic signaling cascades that prevent RGC death from applied insults *in vitro* and from optic neuropathy *in vivo*.[73-75] Supportive neuroprotection to RGC transplants may yield improved survival rates.

Cell transplants are subject to both innate and adaptive immune activity which undermine survival and engraftment. The current study demonstrated that immunosuppression with oral cyclosporine yielded graft survival that was commensurate with that achieved by transplanting into NSG mice which lack adaptive immunity, suggesting that immunological graft rejection (i.e., T cell-mediated immunity) is not a major contributor to hRGC death in the first two weeks following transplantation, but may become a more important factor at later time points. It is likely that innate neuroinflammatory activity plays a greater role in triggering hRGC death early after transplantation. Reactive microgliosis and astrogliosis are known to propagate a neurotoxic cascade in several neurodegenerative conditions including glaucoma.[76,77] Pharmacologic approaches to ameliorating the micro- and macroglial responses to optic neuropathy and RGC transplantation may support enhanced graft survival.[78]

Finally, augmentation of the recipient microenvironment may improve hRGC survival at early time points. The vitreous cavity, where we transplanted hRGCs in this study, is relatively hypoxic and devoid of direct metabolic support for neurons. It is possible that the subset of hRGCs that survive transplantation do so owing to their ability to migrate into the retina where they can obtain metabolic support derived from retinal vascular perfusion. Thus, increasing the early engraftment of donor hRGCs into the host retina may be critical for improving survival. In addition, RGCs are dependent on neurotrophin support, especially during development. Brain-derived neurotrophic factor (BDNF) transported retrogradely from postsynaptic subcortical targets rescues RGCs from developmental apoptosis.[79] BDNF supplementation is neuroprotective to endogenous RGCs following injury,[80,81] and delivery of sustained release BDNF (along with CNTF and GDNF) appears to promote hRGC survival following transplantation.[65] Thus, co-delivery of hRGCs with neurotrophins may improve graft survival at early time points when the neurons are most susceptible to death.

This work has some important limitations. As noted above, the hRGC survival rate at relatively short time points requires improvement. The specific techniques utilized here to bypass the ILM also have important considerations. The developmental ILM dysgenesis model is based on a mutant mouse and is not readily translatable to other species. The use of pronase to enzymatically digest the ILM also comes with relevant experimental limitations. As noted below (methods), we have found that the manufacturer-reported enzymatic activity of pronase does not correlate well to its observed effects in the eye, necessitating that end users either acquire the same lots reported here or perform a lab-specific bioassay to determine the optimal concentration of pronase that will digest the ILM without causing intraocular bleeding, neurotoxicity, or gliotoxicity. It is also worth noting that since the enzymatic activity (U/mg) varies across lots of enzyme, reporting the dose of administered enzyme as a concentration percentage (g/100mL) is uninformative[37] and instead should be reported in terms of U/mL based on lot-specific conversion of enzymatic activity per mg of enzyme. We have documented destructive effects with high doses of intraocular pronase (Fig 1B), and it is likely that concentration drives the differences between the effects of pronase noted here, and elsewhere.[37] Finally, though provocative evidence for functional engraftment is derived from structural localization of hRGC dendrites to the IPL and mobilization of synaptic machinery to those dendrites, electrophysiologic functional assessments are the subject of ongoing work.

Conclusions

Though functional RGC replacement and vision restoration for optic neuropathy is an exciting prospect with high clinical potential, several important hurdles remain. Our work demonstrates that the ILM is a key barrier to the structural engraftment of human stem cell derived RGCs into the host mammalian retina, and that ILM disruption enables a significant proportion of donor RGCs to extend dendrites into the IPL where they may receive presynaptic visual input for eventual communication to the brain. Future work aimed at increasing donor hRGC survival post transplantation, evaluating and modulating hRGC integration into specific retinal circuits, and driving hRGC axonal connectivity to the brain will benefit from ILM disruption as a primary enabling step in the transplantation process.

Materials and Methods

Animals: Adult (8-12 weeks) male and female wild-type C57BL/6J (Jackson strain #664), heterozygous C57BL/6-Tg (CAG-EGFP)1Osb/J (Pan-GFP, Jackson strain #3291), and B6.Cg-Tg(Thy1-YFP)HJrs/J (Thy1-YFP, Jackson Strain #3782) mice were obtained from Jackson Labs (Bar Harbor, USA). Homozygous C57BL/6J-Lama1^{nmf223}/J mice (Jackson strain #5094) were a generous gift from the Edwards Laboratory (Johns Hopkins University). NOD.Cg-*Prkdc*^{scid}*Il2rg*^{tm1Wjl}*/Szj* (NSG, Jackson strain #5557) were obtained from the Johns Hopkins University Research Animal Resources breeding program. All animals were treated in accordance with the ARVO Statement for the Use of Animals in Ophthalmic and Vision Research. All protocols were approved and monitored by the Animal Care Committee of the Johns Hopkins University School of Medicine.

Immunosuppression: Systemic immunosuppression was performed in C57BL/6J, Pan-GFP, and Lama1^{nmf223}/J mice. Cyclosporine solution (Teva, Parsippany, USA) was diluted (210mg/L) in drinking water with 0.5% Kool-Aid to improve flavor and encourage intake and provided *ad libitum*. Body weight was monitored weekly during immunosuppression and noted to be stable.

Enzymatic ILM Disruption: Pronase-E, a nonspecific mixture of endo- and exoproteases from *Streptomyces griseus* (Millipore-Sigma, Burlington, USA, Cat #P8811), was reconstituted in balanced salt solution (BSS) at the indicated concentrations. The manufacturer reported enzymatic activity of pronase is defined such that one unit hydrolyzes casein to produce 1.0 µmole of tyrosine per minute at pH 7.5 and 37°C. However, enzymatic activity depends upon the substrate and the microenvironmental conditions. We found that the intraocular effects of pronase were consistent at specific concentrations of reported enzymatic activity (in U/mL) within given lots, but that similar enzymatic activity concentrations from different lots produced inconsistent effects within the eye. Therefore, rather than rely on manufacturer reported enzymatic activity, we performed a dose-titration bioassay for individual pronase lots. The optimal concentration for lot SLCL6671 was 0.075 U/mL and for SLCK2824 was 1.25 U/mL (Fig 1).

Human pluripotent stem cell culture: H7 hESCs were maintained by clonal propagation in mTeSR1 media (Stem Cell Technologies, Vancouver, USA) on growth factor-reduced Matrigel-coated (BD Biosciences, Franklin Lakes, USA) plates at 37°C in 5 % CO_2. Stem cell colonies were passaged by dissociation with Accutase (Stem Cell Technologies, Vancouver, USA) and re-plating in mTeSR1 media for maintenance with 5 µM blebbistatin (Millipore-Sigma).

hRGC Isolation and Differentiation: Differentiation of H7 hESCs containing the *BRN3B-tdTomato-mThy1.2* was achieved as described previously.[52] In brief, stem cells were dissociated using Accutase and seeded on Matrigel coated plates at a density of 52,600 cm^2 per well in mTeSR1 with 5µM blebbistatin (Millipore-Sigma). After 24h, mTeSR1 was completely exchanged to iNS media consisting of 1:1 Neurobasal and DMEM/F12 media supplemented with 1% N2, and 2% B27. Beginning 24h later, fresh iNS media supplemented with small molecules was exchanged every other day. The working concentrations of small molecules were: Forskolin (FSK, 25µM, Millipore-Sigma). Dorsomorphin (DSM, 1µM, Stem Cell Technologies), Inducer of definitive endoderm 2 (IDE2, 2.5µM, R&D Systems, Minneapolis, USA), DAPT (10µM, Millipore-Sigma), and Nicotinamide (NIC, 10 mM, Millipore-Sigma). DSM and IDE2 were included on days -6, NIC on days 1-10, FSK on days 1-30, and DAPT on days 18-30. Differentiation was induced in 5% CO_2 at 37°C.

Organotypic Retinal Explants: Postmortem human eyes were obtained from Lions Gift of Sight Eyebank (St Paul, Minnesota, USA). Freshly enucleated globes were shipped in glass vials containing saline-moistened gauze on ice and arrived within 24 hours of death. Experiments utilized four retinas from two donors. One donor was a 72-year-old male and the other was an 87-year-old female. Both were Caucasian and neither had known ocular pathology. Human neural retinas were separated from the retinal pigment epithelium and a 5 mm trephine was used to obtain circular samples of tissue from within the macula but excluding the fovea. Peripheral retina and foveal tissue were not evaluated. Mouse neural retinas were isolated immediately following euthanasia and dissected from the retinal pigment epithelium. Four relaxing incisions were placed to flatmount entire murine retinas in Maltese-cross configuration. Both human and mouse retinal explants were flat mounted on polytetrafluoroethylene organotypic filters (Millipore-Sigma) with the photoreceptor side down. Explants were cultured at an air/medium interface and maintained in humidified incubators with 5% CO_2 at 37°C. Media consisted of Neurobasal-A supplemented with 1% N2, 2% B27, 2mM GlutaMAX, 100U/mL penicillin, 100µg/mL streptomycin.[82,83] To disrupt the ILM in organotypic retinal explants, a 2µL droplet of pronase (0.6 U/mL from lot SLCL6671), or BSS (vehicle, negative control) was administered to the inner retinal surface and the culture was incubated for 1 hour.[50,84] The explant was then submersed in ovomucoid (10mg/mL, Millipore-Sigma) and bovine serum albumin (10mg/mL, Millipore-Sigma) for 5 min at 37°C, washed twice in PBS, and then transferred to fresh culture media. To transplant hRGCs onto organotypic retinal explants, a 2 µL droplet of cell suspension, containing 15,000 cells was transferred onto the RGC surface of each explant 24 hours after retinal explant.

RGC Transplantation *in vivo*: Mice were anesthetized with intraperitoneal ketamine (50 mg/kg, Fort Dodge Animal Health, Fort Dodge, IA), xylazine (10 mg/kg, VedCo Inc., Saint Joseph, MO) and acepromazine (2 mg/kg, Phoenix Pharmaceuticals, Burlingame, CA). Pupillary dilation was achieved using 2.5% phenylephrine hydrochloride ophthalmologic eye drops (Akorn, Inc). All procedures were performed under direct visualization using an operating microscope (Carl Zeiss Meditech, Dublin, USA). A drop of 2.5% ophthalmic gel (Goniosoft, OCuSOFT, Rosenberg, USA) was to couple a 4 mm glass contact lens to the cornea and enable direct visualization of the fundus and needle tip, to avoid lens penetration/contact or damage to the retina during intravitreal injection. A 10µL Hamilton syringe and 33-gauge metal needle (Hamilton Co., Reno, USA) were used to deliver 1.5µl of BSS, pronase or RGCs through an injection site 3mm posterior to the superotemporal limbus via a transretinal approach. The needle tip was maintained in the vitreous cavity for 1 minute after injection to allow equilibration of the intraocular pressure and diffusion of the injected solution while minimizing reflux.

Transmission electron microscopy: Animals for TEM were euthanized by exsanguination under general intraperitoneal anesthesia, followed by intracardiac perfusion for 3 minutes with 4% paraformaldehyde in 0.1 M sodium phosphate buffer (Na_3PO_4, pH = 7.2), 1 minute with 0.1M cacodylate buffer, and 7 minutes with 2% paraformaldehyde / 2.5% glutaraldehyde in cacodylate buffer. Eyes were enucleated and kept in fixative overnight. Tissue was post-fixed in 1% osmium tetroxide, dehydrated in ascending alcohol concentrations, and then stained with 1% uranyl acetate in 100% ethanol for 1 hour. Tissues were embedded parallel to the optic axis (longitudinal sections) in an epoxy resin mixture at 60°C for 48 hours. One micrometer thick sections were cut and stained with 1% toluidine blue. Ultra-thin sections (~68nm thick) were collected on copper grids and stained with uranyl acetate and lead citrate before examination with a Hitachi H7600 transmission electron microscope (Hitachi High Technologies, Clarksburg, MD).

Scanning electron microscopy: Animals for SEM were euthanized by overdose of ketamine/xylazine/acepromazine anesthesia followed by cervical dislocation. Retinas were isolated, flat-mounted, and fixed overnight in 2.5% glutaraldehyde, with 3mM $MgCl_2$, in 0.1 M sodium cacodylate buffer (pH 7.2) at 4°C. After buffer rinse, samples were postfixed in 1%

osmium tetroxide in 0.1 M sodium cacodylate buffer for 1h on ice in the dark. Following a dH_2O rinse, samples were dehydrated in a graded series of ethanol and left to dry overnight (in a dessicator) with hexamethyldisilazane (HMDS). Samples were mounted on carbon coated stubs, coated with 15nm of gold-palladium (Denton Desk3) and imaged on a Helios G4 UC focused ion beam SEM (Thermo Fisher Scientific).

Tissue Preparation and Fixation for Confocal Microscopy: Animals were euthanized by ketamine/xylazine/ acepromazine overdose, followed by cervical dislocation. Eyes were enucleated and placed in a Petri dish containing D-PBS (Thermo Fisher Scientific). The anterior segment tissues were removed, and the retina was gently detached from the posterior eyecup. Four radial incisions were made in the retina, and it was flatmounted on 13mm MF-Millipore hydrophilic membrane filters (Millipore-Sigma) in Maltese cross configuration. The retina flatmount was then transferred into a 4% PFA (Electron Microscopy Sciences, Hatfield, USA) solution for one hour at 4°C, and then transferred into PBS at 4°C.

Cryosectioning: Whole eyes were harvested and immerse-fixed in 4% PFA (Electron Microscopy Sciences, Hatfield, USA) at 4°C overnight. Globes were cryoprotected by serial immersion in 5% and 20% sucrose solutions (Millipore-Sigma) for 3 hours each. Globes were then embedded in optimal cutting temperature (OCT) (Sakura Finetek, Torrance, USA) compound and frozen on dry ice. Tissue blocks were stored at -80°C, until use. A cryostat (Leica Microsystems, Wetzlar, Germany) was used to cut transverse sections 18 µm thick, which were thaw-mounted on glass slides.

Immunofluorescence: Retinal flatmounts were washed with PBS for 5 min and then simultaneously blocked and permeabilized in 10% normal goat serum (NGS, Millipore-Sigma) and 0.3% Triton X (Millipore-Sigma) in PBS for 1h at room temperature (RT). Retinal flatmounts were then incubated in primary antibody for 4 days at 4°C on a shaker. Secondary antibody incubations were conducted overnight at 4°C on a shaker. Nuclei were counterstained with DAPI (1:10,000; Millipore-Sigma). Tissue was cover slipped under Aqua-Poly Mount (Polysciences, Warrington, USA) and stored at 4°C in the dark.

Retinal cryosections were washed with PBS and then then blocked and permeabilized in 10% normal goat serum (NGS, Millipore-Sigma) and 0.3% Triton X (Millipore-Sigma) in PBS for 1h at RT, prior to incubation in primary antibody for 24h at 4°C. The sections were then washed with PBS and incubated with corresponding secondary polyclonal goat antibody for 1h at RT. Nuclei were counterstained with DAPI (1:10,000; Millipore-Sigma). Slides were cover slipped using Aqua-Poly Mount (Polysciences).

Primary Antibody	Dilution	Host Species	Source	Catalog #
Brn3a	1:120	Mouse	Millipore Sigma	MAB1585
GFAP	1:1000	Rat	Thermo Fisher	13-0300
Human Mitochondria	1:1000	Mouse	Abcam	Ab92824
Human Nuclei	1:200	Mouse	Millipore Sigma	MAB1281
Laminin	1:1000	Rabbit	Millipore Sigma	L9393
MAP-2	1:1000	Chicken	Novus Biological	NB300-213
mCherry / tdT	1:100	Rat	Thermo Fisher	M11217
Neuronal nuclei	1:800	Mouse	Thermo Fisher	MA5-33103
PKC-α	1:1000	Rabbit	Millipore Sigma	P4334
PSD-95	1:200	Rabbit	Abcam	Ab18258
RBPMS	1:200	Guinea Pig	Phospho Solutions	1832
RFP / tdT	1:400	Rabbit	Rockland	600-401-379
SMI-312	1:200	Mouse	BioLegend	837904
Synaptophysin	1:200	Mouse	Synaptic Systems	101011

Table 1. Primary antibody details for immunofluorescence.

Confocal Microscopy: Retinal flatmounts were examined using a LSM Zeiss 880 Indimo, Axio Examiner confocal microscope (Model 880, Carl Zeiss Microscopy, Thornwood, USA). To obtain high-resolution images of whole retinal flatmount area, images were captured with a large field of view using a Plan-Apochromat 10X/0.45 M27 objective, acquiring full-thickness confocal microscopic z-stacks of retinal flatmount sand using image tiles and stitching to form one single image per sample. The pinhole was set to 1 Airy unit. Scans were obtained in line sequential mode at a pixel dwell time of 1.54µs using bidirectional scanning. Excitation detection wavelengths 488 and 633 shared a single track, whereas excitation wavelengths 405 and 561 had individual tracks to avoid signal bleed-through. Retinas were imaged with the ONH at the center of the tiled mosaic. For high magnification analysis of individual regions of interest, the field of view was manually focused and imaged using the C-Apochromat 40X/1.2 W Korr UV-VIS-IR. Investigators were masked to treatment groups to ensure unbiased field selection for imaging. Unmasking occurred only after microscopy and image analysis.

Quantification of neuronal survival: Quantification of cell survival on retinal flatmounts was performed using the ImageJ (National institute of health, USA) cell counter plugin.[85] NeuN$^+$ bipolar and amacrine cells in the RGCL and PKCα$^+$ rod bipolar cells in the inner nuclear layer were quantified in four quadrants per retina at an eccentricity approximately halfway between the ONH and the retinal edge. Donor tdT$^+$ hRGCs were quantified manually to minimize error, scrolling plane by plane through confocal z-stacks to avoid misinterpretation. All surviving hRGCs were quantified within each retinal flatmount, rather than sampling and extrapolating overall donor neuron survival.

Assessment of donor hRGC soma and neurite integration: The positions of individual hRGC somas were determined to be superficial to, within, or deep to the recipient RGCL using high magnification (40x) confocal z-stacks and Zen software (v8.1.0, 2012 SP1, Carl Zeiss

Microscopy), as previously described. Stack scrolling and orthogonal projections were used to visualize donor hRGC somas and the host RGCL concomitantly, and hRGCs were designated as coplanar with the RGCL only if there was not an endogenous RGC soma deep to the hRGC. Investigators were masked to the identity of treatment groups during image analysis.

Analyses of hRGC neurite localization within the recipient retina were conducted using Imaris (v9.3, Oxford Instruments, Zurich, Switzerland) as previously described.[50,84] High magnification (40x) confocal z-stacks were rendered in 3D, and individual hRGC neurite processes were traced in semi-automated fashion using the filament and autopath tools. Local DAPI staining of the recipient retinal nuclear layers was used to identify neurite localization. The length of neurites within specific retinal layers was quantified using Imaris by segmenting 3D neuronal tracings according to DAPI-registered retinal layer. Quantitative metrics describing the dendritic morphology of structurally integrated hRGCs, such as dendritic density, total branch length, average branch length, maximal branch length, and Sholl analyses (Fig 4) were obtained using Imaris. Investigators were masked to the identity of treatment groups during image analysis.

Statistical Analyses: Data are reported as mean ± SEM unless otherwise stated. Each experiment was performed at least twice. Group means were compared using unpaired non-parametric Mann-Whitney U tests or non-parametric Kruskal Wallis analyses of variance. Following Bonferroni correction for multiple comparisons, $p < 0.05$ was considered statistically significant. Data were analyzed and plotted using Prism (8.0, GraphPad Software, San Diego, USA).

Figure Legends

Figure 1. Proteolytic internal limiting membrane (ILM) disruption and developmental ILM dysgenesis. A) Experimental design assessing retinal histology 2 weeks after intravitreal pronase or BSS (vehicle) injection. B) Gross appearance of mouse retinal flatmounts following intravitreal pronase at several concentrations. Scalebar = 1mm. C) Immunofluorescent labeling of laminin (red) in retinal flatmounts showing an *en face* view of the ILM. Enhanced visualization of intraretinal blood vessels following pronase treatment is artifactual and related to enhanced antibody penetration into the tissue during histological processing. Scalebar = 50 µm. D) Transmission electron microscopy (TEM) of retinal sections at the vitreoretinal interface. Intact ILM, blue arrows; non-compact ILM, red arrows; glia on the retinal surface with overlying ILM breaks, orange arrows; glial protrusions into epiretinal space, green arrows. For additional TEM characterization of *Lama1*^{nmf223} retinas, see Edwards et al.[86] E) Immunofluorescent labeling of laminin (red) in retinal cryosections highlighting the ILM. Scalebar = 50 µm. F) Scanning electron microscopy (SEM) of retinal flatmounts at the ILM. Scalebars = 20 µm. Immunofluorescent labeling of GFAP (G, cyan), neuronal nuclei in the retinal ganglion cell layer (H, maroon) and rod bipolar cells in the inner nuclear layer (I, green) in retinal flatmounts. Scalebars = 50 µm (G-I).

Figure 2. Donor hRGC survival and localization following transplantation in mice. A) Experimental design assessing hRGCs at 2 weeks following transplantation. C57BL/6J mice underwent intravitreal injection of pronase (or BSS, vehicle) 2 weeks prior to transplantation. B) Experimental design assessing hRGCs at 2 weeks following transplantation into *Lama1*^{nmf223} mice. C) Representative retinal flatmounts showing hRGC localization 2 weeks after transplantation. Both ILM disruption (using pronase) and ILM dysgenesis (*Lama1*^{nmf223} recipients) were associated with greater graft dispersion and spontaneous extension of long

neurite projections towards the ONH. Scalebar = 1mm. D) Representative example of a donor hRGC with soma co-planar to the host RGC layer (deep to GFAP$^+$ astrocytes in the RNFL) and neurites extending into the IPL in a *Lama1*^{nmf223} retina. Cell soma and neurite localization was evaluated using a multimodal assessment (see methods). Scalebar = 20 µm. E) Representative example of a donor hRGC with soma and neurites superficial to the RGCL and GFAP$^+$ astrocytes of the RNFL in a C57BL/6J retina with intact ILM. Scalebar = 20 µm. F) Quantification of hRGC survival 2 weeks after transplantation. $^*p<0.05$. G) 3D rendering of confocal z-stack showing *en face* view of 5 hRGCs, one of which has extended dendrites into the IPL (traced in yellow). Scalebar = 30 µm. H) Alternate views of the field shown in G, with DAPI counterstaining of the host retinal nuclear layers, shown with 3D rendering (tracing of integrated hRGC shown in grey) or orthogonal volumetric projections (yellow arrows point to hRGC dendrites in the IPL). Scalebars = 20 µm. I) Quantification of the absolute number and percent of surviving hRGCs which attained somal coplanarity with the host RGCL. J) Quantification of the absolute number and percent of surviving hRGCs which extended dendrites into the IPL. $^*p<0.05$; $^{***}p<0.001$; $^{****}p<0.0001$.

Figure 3. hRGC survival and engraftment following transplantation onto human postmortem organotypic retinal explants. A) Experimental design assessing hRGCs at 1 week following transplantation onto cultured organotypic human postmortem retinal explants. B) Representative retinal flatmounts showing hRGC localization 1 week after co-culture. Scalebar = 1mm. C) Example of several hRGCs in co-culture with human retinal explant. The top panel shows an *en face* view, the bottom panel shows an orthogonal maximum projection through the inner retina. Two of the hRGCs have migrated into the RGC layer and extended neurites into the inner plexiform layer and deeper (arrows). Scalebar = 50µm. Quantification of hRGC survival within co-cultures (D) and the number of hRGCs which extended dendrites into the IPL or deeper (E) are shown. $^{**}p<0.01$.

Figure 4. Morphology of neurites elaborated from donor hRGCs. A) Example of a donor hRGC (red) with soma in the host RGC layer and neurites projecting into the inner plexiform layer (IPL) is shown as an *en face* projection with computational removal of slices superficial to the RGC layer that included other non-integrated hRGCs (left) and as an orthogonal maximum projection (right). Scalebar = 30 µm. B) Examples of endogenous murine RGCs in Thy1-YFP mice demonstrate significantly more complex dendritic arbors (green). Scalebar = 30 µm. C) Examples of hRGC neurite tracings demonstrate heterogeneity and relative simplicity. Scalebar = 100 µm. The length (D) and percentage (E) of hRGC neurites was quantified in a retinal layer-specific manner, demonstrating similar rates of hRGC neurite localization of the RGC layer and IPL. F) Quantitative metrics describing dendritic arbor complexity for endogenous murine RGCs (green) and integrated hRGCs transplanted into pronase-treated (blue) or *Lama1*^{nmf223} (red) retinas demonstrate relative simplicity of hRGC arbors. *$p<0.05$; **$p<0.01$; ***$p<0.001$; ****$p<0.0001$. G) Sholl analysis of the RGCs confirms less complexity in hRGC dendritic arbors. H) hRGCs were noted to extend short, tortuous neurites which morphologically resembled dendrites, and a single lengthy neurite which resembled an axon. Scalebar = 50 µm. I) In most cases, the putative axons grew linearly towards and converged upon the ONH (asterisk). Scalebar = 100 µm. J) 3D rendering of a confocal z-stack centered at the ONH shows hRGC axons (red) diving deeply into the intraocular ONH. Scalebar = 30 µm. K) The number of hRGC axons growing towards the ONH was greatest at approximately 500 µm from the ONH, and higher in retinas where the ILM was disrupted.

Figure 5. Molecular assessment of donor hRGCs. By two weeks following transplantation, hRGCs uniformly expressed RBPMS (A, green) and Brn3a (B, green), markers of a mature RGC phenotype. C) Putative dendrites from hRGCs (magenta), morphologically characterized as short, tortuous neurites near the cell soma, expressed MAP-2 (yellow) but not SMI-312

(cyan). Colocalization of tdT and MAP2 along a linear sample (arrow) is shown. D) Putative axons, morphologically characterized as long linear neurites extending far from the cell soma, expressed SMI-312 (green) but not MAP-2 (not shown). Colocalization along a linear sample is shown. E) Within hRGC dendrites (magenta), colocalization of presynaptic synaptophysin (yellow) and postsynaptic PSD-95 (cyan) were visualized as small puncta. Colocalization of fluorescent signal along four puncta (white lines) are shown. All scalebars = 50 µm.

Figure 6. Assessment for intercellular material transfer. A) Donor hRGCs transplanted into pan-GFP expressing mice uniformly were GFP-negative, confirming their donor origin. Immunofluorescent labeling of human mitochondria (hMito, green), B) and human nuclei (HuNu, green, C) uniformly demonstrated immunoreactivity in donor hRGCs without adjacent labeling of endogenous host RGCs. All scalebars = 25 µm.

Supplemental Figure Legends

Supplemental Figure 1. Widefield view of internal limiting membrane (ILM) integrity and glial morphology in models of ILM disruption. Tiled confocal z-stacks of C57BL/6J mouse retinas treated two weeks earlier with intravitreal BSS (vehicle, A) or pronase (B), and untreated adult *Lama1*^{nmf223} mouse retinas (C) are shown. Immunofluorescent labeling was performed to label the ILM (laminin, red) or retina glia (GFAP, green). Enhanced visualization of laminin^{+} blood vessels in pronase-treated and *Lama1*^{nmf223} retinas is artifactual and related to greater antibody penetration into the retinal tissue during histological processing. Scalebar = 1mm.

Supplemental Figure 2. hRGC survival and engraftment following transplantation onto *Lama1*^{nmf223} murine retinal explants. A) Experimental design assessing hRGCs at 1 week following transplantation onto cultured organotypic C57BL/6J (with intact ILM) or Lama1^{nmf223} mouse retinal explants. B) Example retinal flatmounts showing hRGC localization 1 week after co-culture. Scalebar = 1mm. C) Example of donor hRGCs with somata and neurites superficial to the RGCL and GFAP^{+} astrocytes of the RNFL, with no processes visible within the IPL. Scalebar = 30 µm. D) Example of donor hRGCs with somata co-planar to the host RGC layer (deep to GFAP^{+} astrocytes in the RNFL) and neurites extending into the IPL. Subcellular localization was evaluated using a multimodal assessment (see methods) Scalebar = 30 µm. Quantification of hRGC survival (E) and the rate of dendrite extension into the retinal parenchyma (F) within co-cultures. $^{**}p<0.01$, $^{***}p<0.001$.

Supplemental Figure 3. Comparison of donor hRGC survival following transplantation into immunosuppressed C57BL/6J mice versus immunodeficient NSG mice. A) Experimental design assessing hRGC survival at 2 weeks following transplantation into immunosuppressed C57BL/6J mice or immunodeficient NSG mice. B) Donor hRGC survival was similar between the two recipient groups. C) Example retinal flatmounts showing hRGC localization 2 weeks after transplantation. Scalebar = 1mm.

Supplemental Movies Legends

Supplemental Movie 1: 3D rendering of structurally engrafted hRGC. Movie corresponds to Figure 2G. hRGCs are shown in red and nuclei are counterstained with DAPI in blue. The movie shows temporary computational removal of slices above the RGC layer, which leaves only a single hRGC with soma in the RGC layer and dendrites in the inner plexiform layer. The hRGC is traced (grey) to show localization of the dendritic arbor in 3 dimensions.

Supplemental Movie 2: 3D rendering of structurally engrafted hRGC. Movie shows a second representative example of a structurally engrafted hRGC. hRGCs are shown in red and nuclei are counterstained with DAPI in blue. The movie shows temporary computational removal of slices above the RGC layer, which leaves only a single hRGC with soma in the RGC layer and dendrites in the inner plexiform layer. The hRGC is traced (grey) to show localization of the dendritic arbor in 3 dimensions.

Supplemental Movie 3: 3d rendering of hRGC axons entering the optic nerve head (ONH). hRGC axons are shown in red and nuclei are counterstained with DAPI in blue. The confocal z-stack is centered on the ONH. hRGC axons are traced (grey) to show localization in relation to the ONH in 3 dimensions.

References

1. Zhang N, Wang J, Li Y, Jiang B. Prevalence of primary open angle glaucoma in the last 20 years: a meta-analysis and systematic review. *Scientific Reports.* 2021;11(1):1-12.
2. Varadarajan SG, Hunyara JL, Hamilton NR, Kolodkin AL, Huberman AD. Central nervous system regeneration. *Cell.* 2022;185(1):77-94.
3. Tashiro S, Nishimura S, Iwai H, et al. Functional Recovery from Neural Stem/Progenitor Cell Transplantation Combined with Treadmill Training in Mice with Chronic Spinal Cord Injury. *Sci Rep.* 2016;6:30898.
4. Reidling JC, Relaño-Ginés A, Holley SM, et al. Human Neural Stem Cell Transplantation Rescues Functional Deficits in R6/2 and Q140 Huntington's Disease Mice. *Stem Cell Reports.* 2018;10(1):58-72.
5. Johnson TV, Polo AD, Sahel JA, Schuman JS. Neuroprotection, Neuroenhancement, and Neuroregeneration of the Retina and Optic Nerve. *Ophthalmol Sci.* 2022;2(3):100216.
6. Garita-Hernandez M, Lampič M, Chaffiol A, et al. Restoration of visual function by transplantation of optogenetically engineered photoreceptors. *Nat Commun.* 2019;10(1):4524.
7. Pearson RA, Barber AC, Rizzi M, et al. Restoration of vision after transplantation of photoreceptors. *Nature.* 2012;485(7396):99-103.
8. Eiraku M, Takata N, Ishibashi H, et al. Self-organizing optic-cup morphogenesis in three-dimensional culture. *Nature.* 2011;472(7341):51-56.
9. Sluch VM, Chamling X, Liu MM, et al. Enhanced Stem Cell Differentiation and Immunopurification of Genome Engineered Human Retinal Ganglion Cells. *Stem Cell Transl Med.* 2017;6(11):1972-1986.
10. Rabesandratana O, Chaffiol A, Mialot A, et al. Generation of a Transplantable Population of Human iPSC-Derived Retinal Ganglion Cells. *Front Cell Dev Biol.* 2020;8:585675.
11. Ji SL, Tang SB. Differentiation of retinal ganglion cells from induced pluripotent stem cells: a review. *Int J Ophthalmol.* 2019;12(1):152-160.
12. Tanaka T, Yokoi T, Tamalu F, Watanabe S, Nishina S, Azuma N. Generation of retinal ganglion cells with functional axons from human induced pluripotent stem cells. *Sci Rep.* 2015;5:8344.
13. Williams PR, Benowitz LI, Goldberg JL, He Z. Axon Regeneration in the Mammalian Optic Nerve. *Annu Rev Vis Sci.* 2020;6:195-213.
14. Duan X, Qiao M, Bei F, Kim IJ, He Z, Sanes JR. Subtype-specific regeneration of retinal ganglion cells following axotomy: effects of osteopontin and mTOR signaling. *Neuron.* 2015;85(6):1244-1256.
15. Leibinger M, Andreadaki A, Diekmann H, Fischer D. Neuronal STAT3 activation is essential for CNTF- and inflammatory stimulation-induced CNS axon regeneration. *Cell Death & Disease.* 2013;4.
16. Zhang Y, Williams PR, Jacobi A, et al. Elevating Growth Factor Responsiveness and Axon Regeneration by Modulating Presynaptic Inputs. *Neuron.* 2019;103(1):39-51 e35.
17. Bray ER, Yungher BJ, Levay K, et al. Thrombospondin-1 Mediates Axon Regeneration in Retinal Ganglion Cells. *Neuron.* 2019;103(4):642-657 e647.
18. Park KK, Liu K, Hu Y, et al. Promoting axon regeneration in the adult CNS by modulation of the PTEN/mTOR pathway. *Science.* 2008;322(5903):963-966.
19. Smith PD, Sun F, Park KK, et al. SOCS3 deletion promotes optic nerve regeneration in vivo. *Neuron.* 2009;64(5):617-623.

20. Sun F, Park KK, Belin S, et al. Sustained axon regeneration induced by co-deletion of PTEN and SOCS3. *Nature.* 2011;480(7377):372-375.
21. Moore DL, Blackmore MG, Hu Y, et al. KLF family members regulate intrinsic axon regeneration ability. *Science.* 2009;326(5950):298-301.
22. Lindborg JA, Tran NM, Chenette DM, et al. Optic nerve regeneration screen identifies multiple genes restricting adult neural repair. *Cell Rep.* 2021;34(9):108777.
23. Yin YQ, Henzl MT, Lorber B, et al. Oncomodulin is a macrophage-derived signal for axon regeneration in retinal ganglion cells. *Nat Neurosci.* 2006;9(6):843-852.
24. de Lima S, Koriyama Y, Kurimoto T, et al. Full-length axon regeneration in the adult mouse optic nerve and partial recovery of simple visual behaviors. *P Natl Acad Sci USA.* 2012;109(23):9149-9154.
25. Wang J, He XL, Meng HY, et al. Robust Myelination of Regenerated Axons Induced by Combined Manipulations of GPR17 and Microglia. *Neuron.* 2020;108(5):876-+.
26. Lim JH, Stafford BK, Nguyen PL, et al. Neural activity promotes long-distance, target-specific regeneration of adult retinal axons. *Nat Neurosci.* 2016;19(8):1073-1084.
27. Bei F, Lee HHC, Liu X, et al. Restoration of Visual Function by Enhancing Conduction in Regenerated Axons. *Cell.* 2016;164(1-2):219-232.
28. Benowitz LI, He Z, Goldberg JL. Reaching the brain: Advances in optic nerve regeneration. *Exp Neurol.* 2017;287(Pt 3):365-373.
29. de Lima S, Koriyama Y, Kurimoto T, et al. Full-length axon regeneration in the adult mouse optic nerve and partial recovery of simple visual behaviors. *Proc Natl Acad Sci U S A.* 2012;109(23):9149-9154.
30. Mead B, Logan A, Berry M, Leadbeater W, Scheven BA. Intravitreally transplanted dental pulp stem cells promote neuroprotection and axon regeneration of retinal ganglion cells after optic nerve injury. *Investigative ophthalmology & visual science.* 2013;54(12):7544-7556.
31. Mead B, Amaral J, Tomarev S. Mesenchymal Stem Cell-Derived Small Extracellular Vesicles Promote Neuroprotection in Rodent Models of Glaucoma. *Investigative ophthalmology & visual science.* 2018;59(2):702-714.
32. Johnson TV, DeKorver NW, Levasseur VA, et al. Identification of retinal ganglion cell neuroprotection conferred by platelet-derived growth factor through analysis of the mesenchymal stem cell secretome. *Brain.* 2014;137:503-519.
33. Johnson TV, Bull ND, Hunt DP, Marina N, Tomarev SI, Martin KR. Neuroprotective Effects of Intravitreal Mesenchymal Stem Cell Transplantation in Experimental Glaucoma. *Investigative Ophthalmology & Visual Science.* 2010;51(4):2051-2059.
34. Venugopalan P, Wang Y, Nguyen T, Huang A, Muller KJ, Goldberg JL. Transplanted neurons integrate into adult retinas and respond to light. *Nature communications.* 2016;7:10472.
35. Wu YR, Hashiguchi T, Sho J, Chiou SH, Takahashi M, Mandai M. Transplanted Mouse Embryonic Stem Cell-Derived Retinal Ganglion Cells Integrate and Form Synapses in a Retinal Ganglion Cell-Depleted Mouse Model. *Invest Ophthalmol Vis Sci.* 2021;62(13):26.
36. Oswald J, Kegeles E, Minelli T, Volchkov P, Baranov P. Transplantation of miPSC/mESC-derived retinal ganglion cells into healthy and glaucomatous retinas. *Mol Ther Methods Clin Dev.* 2021;21:180-198.
37. Vrathasha V, Nikonov S, Bell BA, et al. Transplanted human induced pluripotent stem cells- derived retinal ganglion cells embed within mouse retinas and are electrophysiologically functional. *iScience.* 2022;25(11):105308.
38. Zhang KY, Aguzzi EA, Johnson TV. Retinal Ganglion Cell Transplantation: Approaches for Overcoming Challenges to Functional Integration. *Cells.* 2021;10(6).

39. Tavakoli S, Peynshaert K, Lajunen T, et al. Ocular barriers to retinal delivery of intravitreal liposomes: Impact of vitreoretinal interface. *Journal of controlled release : official journal of the Controlled Release Society.* 2020;328:952-961.
40. Dalkara D, Kolstad KD, Guerin KI, et al. AAV mediated GDNF secretion from retinal glia slows down retinal degeneration in a rat model of retinitis pigmentosa. *Mol Ther.* 2011;19(9):1602-1608.
41. Halfter W, Dong S, Dong A, Eller AW, Nischt R. Origin and turnover of ECM proteins from the inner limiting membrane and vitreous body. *Eye (Lond).* 2008;22(10):1207-1213.
42. Semeraro F, Morescalchi F, Duse S, Gambicorti E, Russo A, Costagliola C. Current Trends about Inner Limiting Membrane Peeling in Surgery for Epiretinal Membranes. *J Ophthalmol.* 2015;2015:671905.
43. Sun LO, Brady CM, Cahill H, et al. Functional assembly of accessory optic system circuitry critical for compensatory eye movements. *Neuron.* 2015;86(4):971-984.
44. Edwards MM, Mammadova-Bach E, Alpy F, et al. Mutations in Lama1 disrupt retinal vascular development and inner limiting membrane formation. *The Journal of biological chemistry.* 2010;285(10):7697-7711.
45. Edwards MM, McLeod DS, Grebe R, Heng C, Lefebvre O, Lutty GA. Lama1 mutations lead to vitreoretinal blood vessel formation, persistence of fetal vasculature, and epiretinal membrane formation in mice. *BMC developmental biology.* 2011;11:60.
46. Gelman R, Stevenson W, Prospero Ponce C, Agarwal D, Christoforidis JB. Retinal Damage Induced by Internal Limiting Membrane Removal. *J Ophthalmol.* 2015;2015:939748.
47. Chawla R, Tripathy K, Temkar S, Kumar V. Internal limiting membrane: The innermost retinal barrier. *Med Hypotheses.* 2017;98:60-62.
48. Kurimoto Y, Shibuki H, Kaneko Y, et al. Transplantation of adult rat hippocampus-derived neural stem cells into retina injured by transient ischemia. *Neurosci Lett.* 2001;306(1-2):57-60.
49. Miltner AM, La Torre A. Retinal Ganglion Cell Replacement: Current Status and Challenges Ahead. *Dev Dyn.* 2019;248(1):118-128.
50. Zhang KY, Tuffy C, Mertz JL, et al. Role of the Internal Limiting Membrane in Structural Engraftment and Topographic Spacing of Transplanted Human Stem Cell-Derived Retinal Ganglion Cells. *Stem cell reports.* 2021;16(1):149-167.
51. Johnson TV, Bull ND, Martin KR. Identification of barriers to retinal engraftment of transplanted stem cells. *Investigative ophthalmology & visual science.* 2010;51(2):960-970.
52. Sluch VM, Chamling X, Liu MM, et al. Enhanced Stem Cell Differentiation and Immunopurification of Genome Engineered Human Retinal Ganglion Cells. *Stem Cells Transl Med.* 2017;6(11):1972-1986.
53. Radaelli E, Santagostino SF, Sellers RS, Brayton CF. Immune Relevant and Immune Deficient Mice: Options and Opportunities in Translational Research. *ILAR J.* 2018;59(3):211-246.
54. Peynshaert K, Devoldere J, Minnaert AK, De Smedt SC, Remaut K. Morphology and Composition of the Inner Limiting Membrane: Species-Specific Variations and Relevance toward Drug Delivery Research. *Curr Eye Res.* 2019;44(5):465-475.
55. Sluch VM, Davis C-hO, Ranganathan V, et al. Differentiation of human ESCs to retinal ganglion cells using a CRISPR engineered reporter cell line. *Scientific reports.* 2015;5:16595.
56. Pearson RA, Gonzalez-Cordero A, West EL, et al. Donor and host photoreceptors engage in material transfer following transplantation of post-mitotic photoreceptor precursors. *Nat Commun.* 2016;7:13029.

57. Nickerson PEB, Ortin-Martinez A, Wallace VA. Material Exchange in Photoreceptor Transplantation: Updating Our Understanding of Donor/Host Communication and the Future of Cell Engraftment Science. *Front Neural Circuits.* 2018;12:17.
58. Kalargyrou AA, Basche M, Hare A, et al. Nanotube-like processes facilitate material transfer between photoreceptors. *EMBO Rep.* 2021;22(11):e53732.
59. Heisterkamp P, Borsch O, Lezama ND, et al. Evidence for endogenous exchange of cytoplasmic material between a subset of cone and rod photoreceptors within the adult mammalian retina via direct cell-cell connections. *Exp Eye Res.* 2022;219:109033.
60. Boudreau-Pinsonneault C, Cayouette M. Cell lineage tracing in the retina: Could material transfer distort conclusions? *Dev Dyn.* 2018;247(1):10-17.
61. Zhang X, Tenerelli K, Wu S, et al. Cell transplantation of retinal ganglion cells derived from hESCs. *Restorative Neurology & Neuroscience.* 2020;38(2):131-140.
62. Divya MS, Rasheed VA, Schmidt T, Lalitha S, Hattar S, James J. Intraocular Injection of ES Cell-Derived Neural Progenitors Improve Visual Function in Retinal Ganglion Cell-Depleted Mouse Models. *Front Cell Neurosci.* 2017;11:295.
63. Li K, Zhong X, Yang S, et al. HiPSC-derived retinal ganglion cells grow dendritic arbors and functional axons on a tissue-engineered scaffold. *Acta biomaterialia.* 2017;54:117-127.
64. Luo Z, Chang KC, Wu S, et al. Directly induced human retinal ganglion cells mimic fetal RGCs and are neuroprotective after transplantation in vivo. *Stem Cell Reports.* 2022.
65. Soucy JR, Todd L, Kriukov E, Phay M, Reh TA, Baranov P. Introduced chemokine gradients guide transplanted and regenerated retinal neurons toward their natural position in the retina. *bioRxiv.* 2022.
66. Far PM, Yeung SC, Ma PE, et al. Effects of Internal Limiting Membrane Peel for Idiopathic Epiretinal Membrane Surgery: A Systematic Review of Randomized Controlled Trials. *Am J Ophthalmol.* 2021;231:79-87.
67. Wang Y, Zhao X, Zhang W, Yang J, Chen Y. FOVEA-SPARING VERSUS COMPLETE INTERNAL LIMITING MEMBRANE PEELING IN VITRECTOMY FOR VITREOMACULAR INTERFACE DISEASES: A Systematic Review and Meta-Analysis. *Retina.* 2021;41(6):1143-1152.
68. Riccomagno MM, Sun LO, Brady CM, et al. Cas adaptor proteins organize the retinal ganglion cell layer downstream of integrin signaling. *Neuron.* 2014;81(4):779-786.
69. Gamlin PD, Alexander JJ, Boye SL, Witherspoon CD, Boye SE. SubILM Injection of AAV for Gene Delivery to the Retina. *Methods Mol Biol.* 2019;1950:249-262.
70. Peynshaert K, Devoldere J, Minnaert A-K, De Smedt SC, Remaut K. Morphology and Composition of the Inner Limiting Membrane: Species-Specific Variations and Relevance toward Drug Delivery Research. *Current Eye Research.* 2019;44(5):465-475.
71. Yang S-G, Li C-P, Peng X-Q, Teng Z-Q, Liu C-M, Zhou F-Q. Strategies to Promote Long-Distance Optic Nerve Regeneration. *Frontiers in cellular neuroscience.* 2020;14:119-119.
72. Rytomaa M, Martins LM, Downward J. Involvement of FADD and caspase-8 signalling in detachment-induced apoptosis. *Curr Biol.* 1999;9(18):1043-1046.
73. Welsbie DS, Yang ZY, Ge Y, et al. Functional genomic screening identifies dual leucine zipper kinase as a key mediator of retinal ganglion cell death. *Proceedings of the National Academy of Sciences of the United States of America.* 2013;110(10):4045-4050.
74. Welsbie DS, Mitchell KL, Jaskula-Ranga V, et al. Enhanced Functional Genomic Screening Identifies Novel Mediators of Dual Leucine Zipper Kinase-Dependent Injury Signaling in Neurons. *Neuron.* 2017;94(6):1142-+.

75. Patel AK, Broyer RM, Lee CD, et al. Inhibition of GCK-IV kinases dissociates cell death and axon regeneration in CNS neurons. *Proceedings of the National Academy of Sciences of the United States of America.* 2020;117(52):33597-33607.
76. Liddelow SA, Guttenplan KA, Larke LEC, et al. Neurotoxic reactive astrocytes are induced by activated microglia. *Nature.* 2017;541(7638):481-487.
77. Zhao XH, Sun R, Luo XT, Wang F, Sun XD. The Interaction Between Microglia and Macroglia in Glaucoma. *Frontiers in Neuroscience.* 2021;15.
78. Sterling JK, Adetunji MO, Guttha S, et al. GLP-1 Receptor Agonist NLY01 Reduces Retinal Inflammation and Neuron Death Secondary to Ocular Hypertension. *Cell Reports.* 2020;33(5).
79. Ma YT, Hsieh T, Forbes ME, Johnson JE, Frost DO. BDNF injected into the superior colliculus reduces developmental retinal ganglion cell death. *Journal of Neuroscience.* 1998;18(6):2097-2107.
80. Khatib TZ, Osborne A, Yang S, et al. Receptor-ligand supplementation via a self-cleaving 2A peptide-based gene therapy promotes CNS axonal transport with functional recovery. *Science Advances.* 2021;7(14).
81. Osborne A, Khatib TZ, Songra L, et al. Neuroprotection of retinal ganglion cells by a novel gene therapy construct that achieves sustained enhancement of brain-derived neurotrophic factor/tropomyosin- related kinase receptor-B signaling. *Cell Death & Disease.* 2018;9.
82. Johnson TV, Martin KR. Development and characterization of an adult retinal explant organotypic tissue culture system as an in vitro intraocular stem cell transplantation model. *Invest Ophthalmol Vis Sci.* 2008;49(8):3503-3512.
83. Johnson TV, Oglesby EN, Steinhart MR, Cone-Kimball E, Jefferys J, Quigley HA. Time-Lapse Retinal Ganglion Cell Dendritic Field Degeneration Imaged in Organotypic Retinal Explant Culture. *Invest Ophthalmol Vis Sci.* 2016;57(1):253-264.
84. Zhang KY, Johnson TV. Analyses of transplanted human retinal ganglion cell morphology and localization in murine organotypic retinal explant culture. *STAR Protoc.* 2022;3(2):101328.
85. Schindelin J, Arganda-Carreras I, Frise E, et al. Fiji: an open-source platform for biological-image analysis. *Nat Methods.* 2012;9(7):676-682.
86. Edwards MM, McLeod DS, Grebe R, Heng C, Lefebvre O, Lutty GA. Lama1 mutations lead to vitreoretinal blood vessel formation, persistence of fetal vasculature, and epiretinal membrane formation in mice. *BMC Dev Biol.* 2011;11:60.

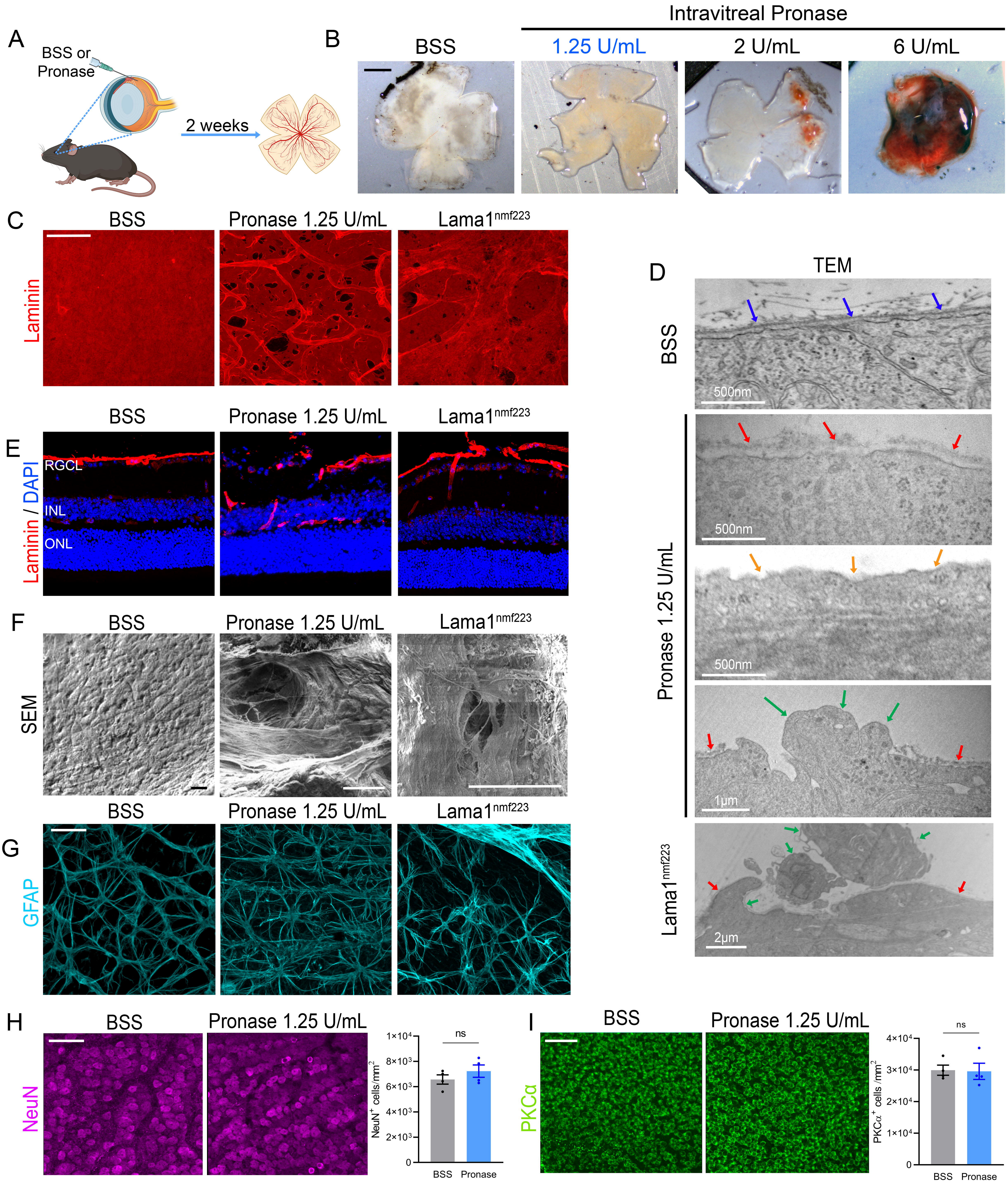
A
BSS or Pronase
2 weeks
B
Intravitreal Pronase
BSS
1.25 U/mL
2 U/mL
6 U/mL
C
BSS
Pronase 1.25 U/mL
Lama1nmf223
Laminin
D
TEM
BSS
500nm
Pronase 1.25 U/mL
500nm
500nm
1μm
Lama1nmf223
2μm
E
BSS
Pronase 1.25 U/mL
Lama1nmf223
Laminin / DAPI
RGCL
INL
ONL
F
BSS
Pronase 1.25 U/mL
Lama1nmf223
SEM
G
BSS
Pronase 1.25 U/mL
Lama1nmf223
GFAP
H
BSS
Pronase 1.25 U/mL
NeuN
NeuN+ cells/mm2
1×10⁴
8×10³
6×10³
4×10³
2×10³
0
ns
BSS
Pronase
I
BSS
Pronase 1.25 U/mL
PKCα
PKCα+ cells /mm2
4×10⁴
3×10⁴
2×10⁴
1×10⁴
0
ns
BSS
Pronase

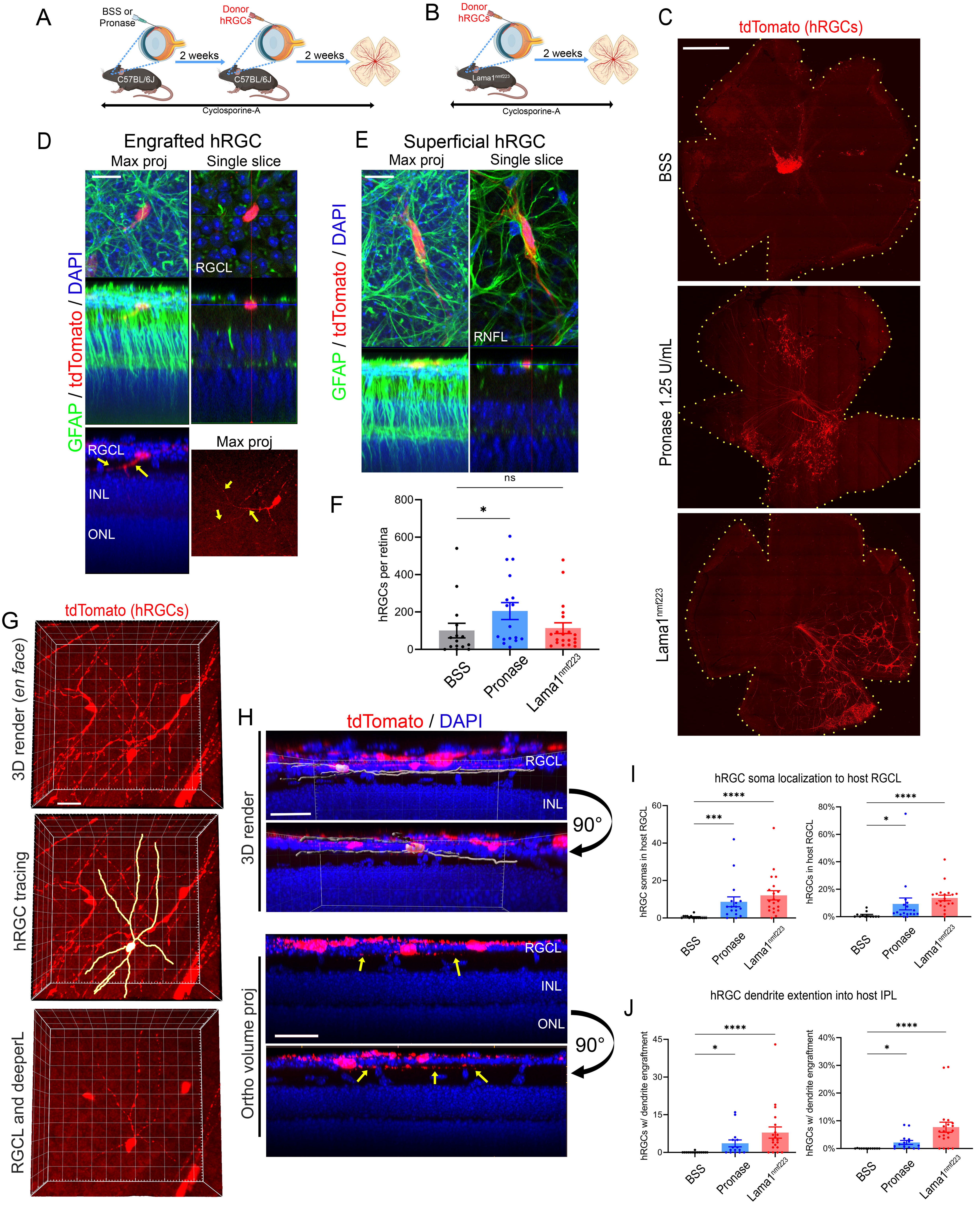
A
BSS or Pronase
Donor hRGCs
2 weeks
2 weeks
C57BL/6J
C57BL/6J
Cyclosporine-A
B
Donor hRGCs
2 weeks
Lama1nmf223
Cyclosporine-A
C
tdTomato (hRGCs)
BSS
Pronase 1.25 U/mL
Lama1nmf223
D
Engrafted hRGC
Max proj
Single slice
GFAP / tdTomato / DAPI
RGCL
RGCL
INL
ONL
Max proj
E
Superficial hRGC
Max proj
Single slice
GFAP / tdTomato / DAPI
RNFL
F
hRGCs per retina
800
600
400
200
0
ns
*
BSS
Pronase
Lama1nmf223
G
tdTomato (hRGCs)
3D render (en face)
hRGC tracing
RGCL and deeperL
H
tdTomato / DAPI
3D render
RGCL
INL
90°
Ortho volume proj
RGCL
INL
ONL
90°
I
hRGC soma localization to host RGCL
hRGC somas in host RGCL
60
40
20
0
***
****
BSS
Pronase
Lama1nmf223
hRGCs in host RGCL
80%
60%
40%
20%
0%
*
****
BSS
Pronase
Lama1nmf223
J
hRGC dendrite extention into host IPL
hRGCs w/ dendrite engraftment
45
30
15
0
*
****
BSS
Pronase
Lama1nmf223
hRGCs w/ dendrite engraftment
40%
30%
20%
10%
0%
*
****
BSS
Pronase
Lama1nmf223

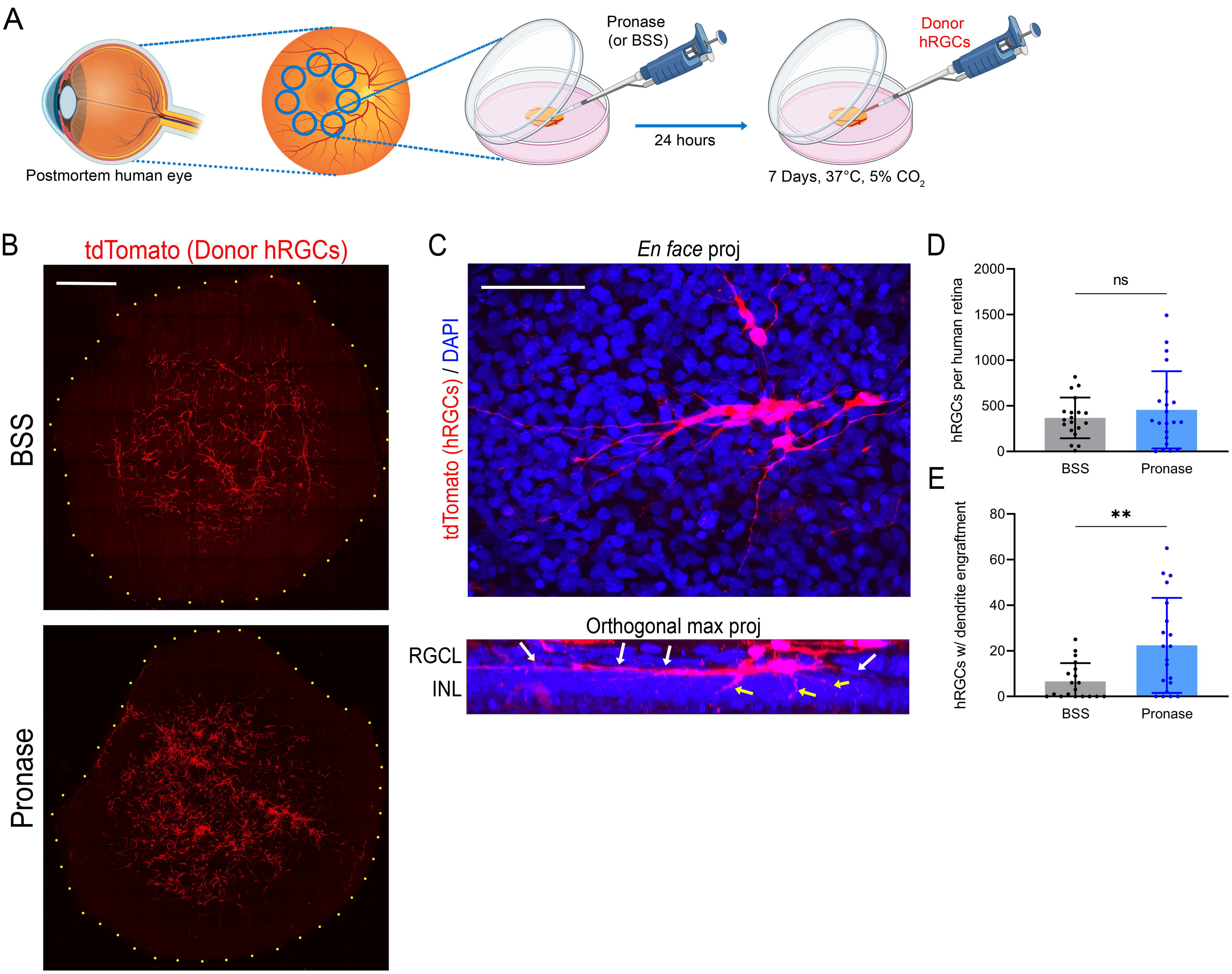
A
Postmortem human eye
Pronase
(or BSS)
24 hours
Donor
hRGCs
7 Days, 37°C, 5% CO_2
B
tdTomato (Donor hRGCs)
BSS
Pronase
C
En face proj
tdTomato (hRGCs) / DAPI
Orthogonal max proj
RGCL
INL
D
hRGCs per human retina
2000
1500
1000
500
0
ns
BSS
Pronase
E
hRGCs w/ dendrite engraftment
80
60
40
20
0
**
BSS
Pronase

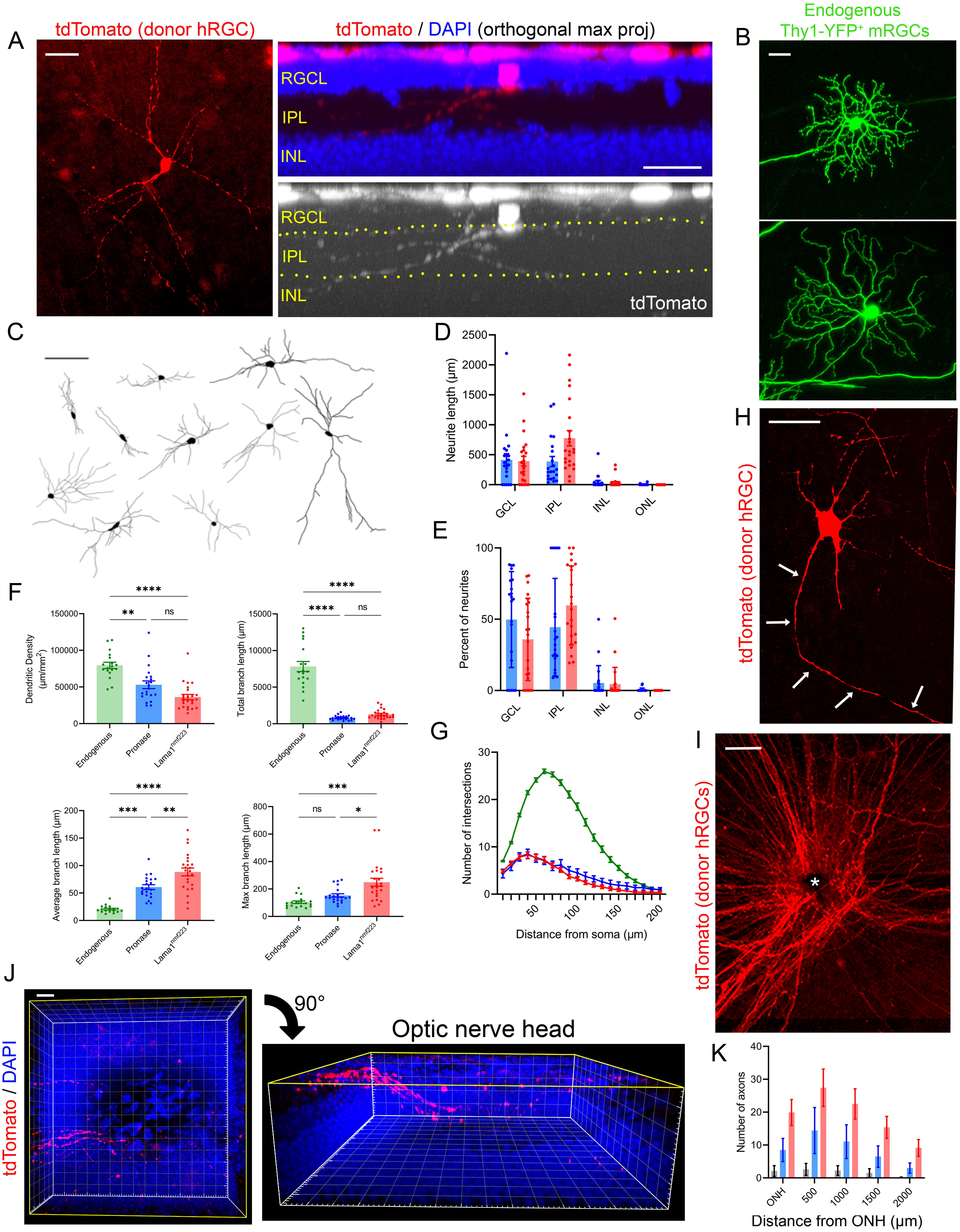
A
tdTomato (donor hRGC)
tdTomato / DAPI (orthogonal max proj)
RGCL
IPL
INL
RGCL
IPL
INL
tdTomato
B
Endogenous
Thy1-YFP⁺ mRGCs
C
D
Neurite length (µm)
2500
2000
1500
1000
500
0
GCL
IPL
INL
ONL
E
Percent of neurites
100
50
0
GCL
IPL
INL
ONL
F
Dendritic Density (µm/mm²)
150000
100000
50000
0
****
**
ns
Endogenous
Pronase
Lama1nmf223
Total branch length (µm)
15000
10000
5000
0
****
****
ns
Endogenous
Pronase
Lama1nmf223
Average branch length (µm)
200
150
100
50
0
****
***
**
Endogenous
Pronase
Lama1nmf223
Max branch length (µm)
800
600
400
200
0
***
ns
*
Endogenous
Pronase
Lama1nmf223
G
Number of intersections
30
20
10
0
50
100
150
200
Distance from soma (µm)
H
tdTomato (donor hRGC)
I
tdTomato (donor hRGCs)
*
J
tdTomato / DAPI
90°
Optic nerve head
K
Number of axons
40
30
20
10
0
ONH
500
1000
1500
2000
Distance from ONH (µm)

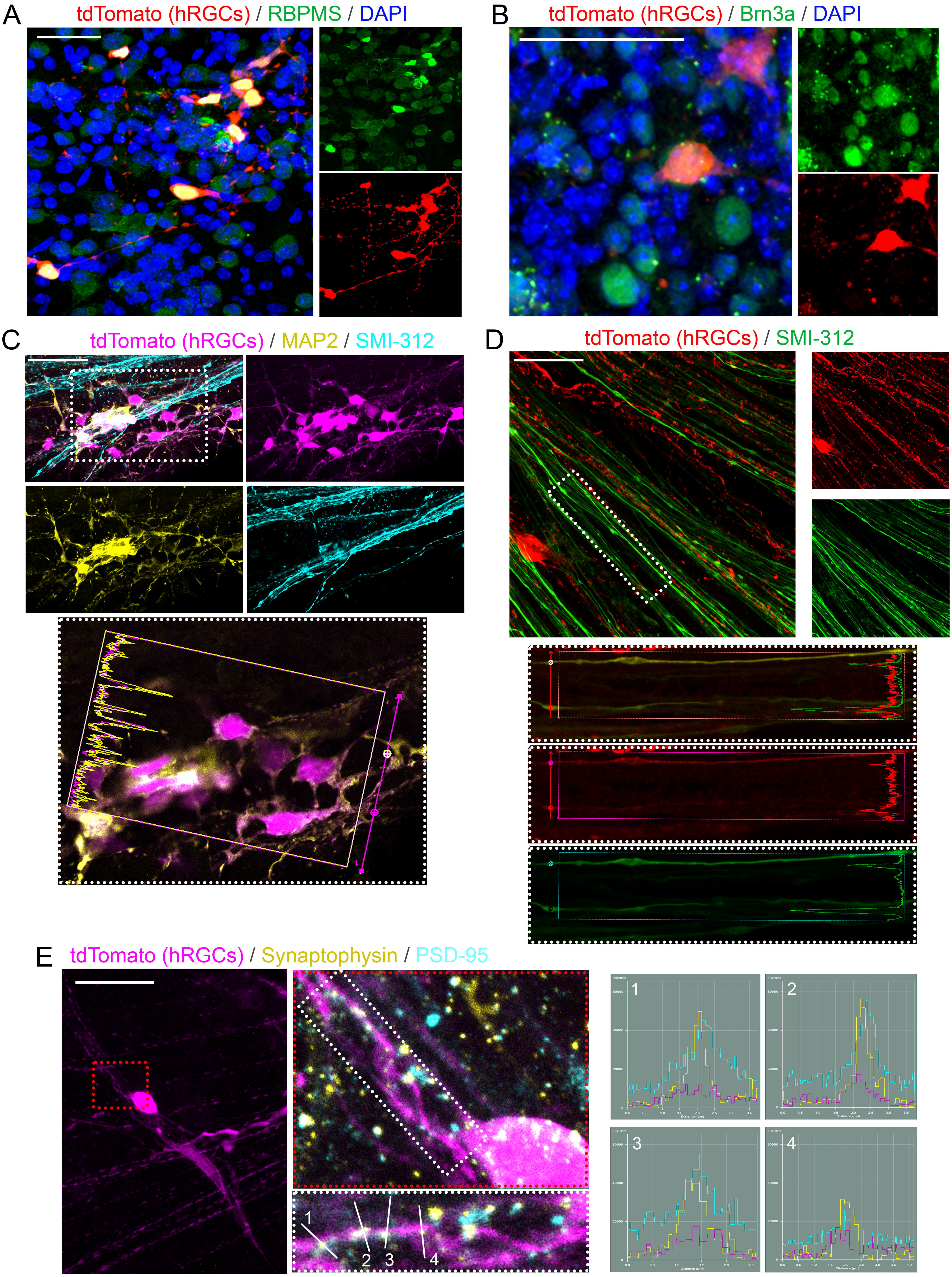
A
tdTomato (hRGCs) / RBPMS / DAPI
B
tdTomato (hRGCs) / Brn3a / DAPI
C
tdTomato (hRGCs) / MAP2 / SMI-312
D
tdTomato (hRGCs) / SMI-312
E
tdTomato (hRGCs) / Synaptophysin / PSD-95
1
2
3
4
Intensity
Distance (µm)

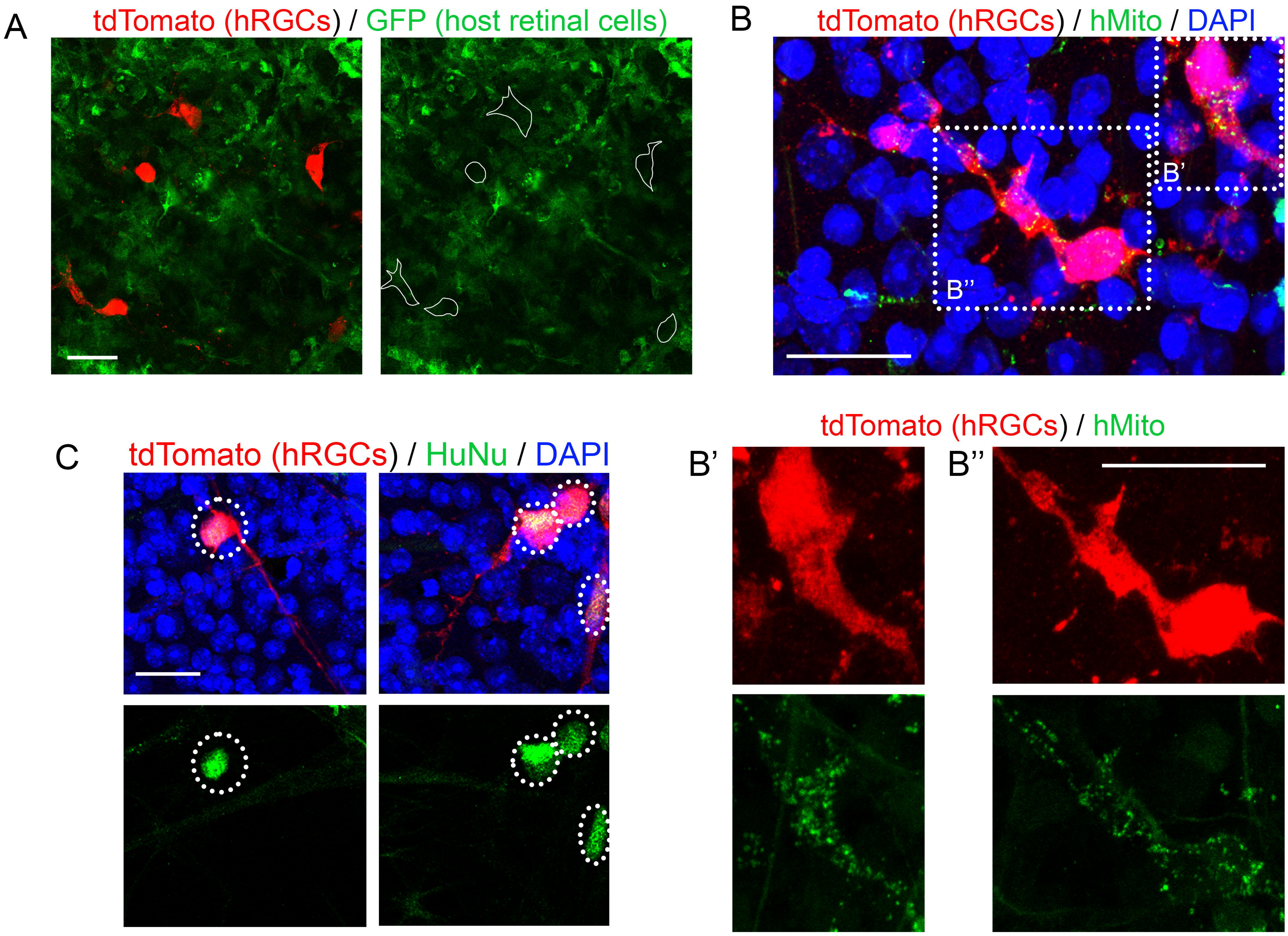
A
tdTomato (hRGCs) / GFP (host retinal cells)
B
tdTomato (hRGCs) / hMito / DAPI
B'
B''
C
tdTomato (hRGCs) / HuNu / DAPI
tdTomato (hRGCs) / hMito
B'
B''